(2)

MICROSTRUCTURE-BASED FATIGUE LIFE PREDICTION METHODS FOR NAVAL STEEL STRUCTURES

Quarterly Report
January 30, 1993

SwRI Project No. 06-4414
ONR Contract No. N00014-91-C-0214

Submitted To:

Dr. A. K. Vasudévan
Office of Naval Research
800 N. Quincy Street
Arlington, VA 22217-5000

Prepared By:

K. S. Chan
R. C. McClung
T. Y. Torng

SOUTHWEST RESEARCH INSTITUTE
San Antonio, TX Houston, TX Detroit, MI Washington, DC

Introduction

The ongoing development of new HSLA (high-strength, low alloy) steels for use in ship and submarine structures permits increases in design stress levels, which may in turn increase the significance of fatigue cracking as a threat to structural integrity. The subject program has been motivated by the desire for improved understandings of the relationships between microstructure and fatigue damage in naval steel structures, with particular application to the prediction of fatigue life. Among the intended products of the study are improved methods for fatigue life prediction which give appropriate attention to different potential microstructures and associated microstructural influences on fatigue crack initiation and growth rates. The methods could be used to provide guidance in optimizing alloy chemistry, processing, and welding protocols for improved fatigue resistance, while also expediting improved fitness-for-service assessments of actual or postulated cracking.

The basic technical approach has been first to identify the rate-controlling fatigue mechanisms and characterize the relevant microstructures for microcrack nucleation and growth. These studies have been informed by a series of critical quantitative experiments in which fatigue microcracks were nucleated and grown through microstructures of interest. The goal is to establish quantitative relationships between microstructural and loading parameters and fatigue damage. The second key step is then to develop practical engineering expressions to predict total *S-N* fatigue life which incorporate these microstructure-load-damage relationships. These life prediction models are to be expressed in an appropriate probabilistic framework which enables a quantitative assessment of the probability of *S-N* failure at a performance level of interest as a function of uncertainties in material/load/geometry input parameters.

The focus of the first year (ending July 1992, and summarized in the First Annual Report) was on experimental observations of fatigue damage in different microstructures for HSLA steels. Experimental methods were developed to study microcrack nucleation and growth with *S-N* fatigue specimens. Microstructures were modified with various heat treatments and characterized with appropriate optical and electron microscopies. Results suggested that the *S-N* fatigue life could be adequately characterized in terms of the nucleation and growth of individual microcracks. Crack nucleation was found to be significantly dependent on microstructure, but the nucleation phase was typically a small fraction of the total life. Microcrack growth rates appeared to be only mildly dependent on microstructure, which is consistent with available data on large crack growth rates. The growth rate was relatively insensitive to the ferrite matrix morphology, but may have been affected by the size, volume fraction, and perhaps mean free path of the fine copper precipitates.

In our Annual Letter Report for FY92, we identified a series of critical questions to guide our future work. In this quarterly progress report, we will briefly discuss how we have addressed these critical questions during the past few months.

Large Cracks vs. Microcracks

One basic question was whether a fundamental difference existed between fatigue crack growth rates for microcracks and large cracks in HSLA-80. Comparisons of our microcrack growth rate data with large crack data from Lehigh researchers on the same heat of material and with other large crack growth data from the literature suggest that the differences are relatively minor, although microcrack growth may occur at applied stress intensity factor ranges smaller than the large crack threshold value. However, we have not been able to draw a firm conclusion because of a shortage of large crack data at very low growth rates (i.e., very near threshold). Our colleagues at Lehigh

have informed us that they still intend to generate these data with our common material and provide us with the results. We have chosen to postpone our final analysis/comparison of large crack and microcrack growth rates until additional near-threshold data are available.

Microstructural Issues

The previous list of critical questions included three topics related to microstructural issues: the influence of copper precipitate size and spacing; a rigorous evaluation of microstructural influences on microcrack nucleation and growth in HSLA-80 steels, along with the development of appropriate scaling laws; and the development of specific equations which can be integrated to give good estimates of S-N fatigue life. We have made substantial progress in answering these questions, although some further work remains. A detailed discussion of these advances is presented in the manuscript, "Scaling Laws for Fatigue Crack Growth in Steels," which is enclosed as an attachment to this quarterly report. This manuscript is being submitted for publication to *Metallurgical Transactions A*. A brief summary is provided here.

A set of scaling laws has been developed for describing both intermittent and continuous fatigue crack growth in steels in the power-law regime. The proposed scaling laws are developed on the basis that fatigue crack growth occurs as the result of low-cycle fatigue failure of a crack-tip element whose width and height correspond to the dislocation cell size and barrier spacing, respectively. The results show that the effects of microstructure can be described entirely in terms of a dimensionless microstructural parameter, ξ, which is defined in terms of yield stress, fatigue ductility, dislocation cell size, and dislocation barrier spacing. For both discontinuous and continuum crack growth, the crack extension rate, da/dN, scales with ξ and $\Delta K/E$, where ΔK is the stress intensity range and E is Young's modulus. Application of the model to HSLA and conventional ferritic, ferritic/pearlitic, and martensitic steels reveals that the lack of a strong microstructural influence on fatigue crack growth in the power-law regime is due to increasing yield stress and fatigue ductility with decreasing dislocation barrier spacing, which leads to a narrow range of ξ values and crack growth rates. Variations of da/dN data with microstructure in HSLA-80 steels, including the effects of copper precipitates, are explained in terms of the proposed model.

The development of these scaling laws for large cracks represents the first substantial step towards developing specific microcrack nucleation and growth equations which can be integrated to give good estimates of *S-N* fatigue life. The final form of these equations will be developed in conjunction with ongoing research on stochastic modeling, which is described next. These scaling laws do not specifically address the issue of near-threshold growth rates. We will evaluate the significance of that issue following further investigation of the large crack vs. microcrack issue, described above.

Stochastic Modeling

Fatigue crack growth is fundamentally a random phenomenon because of the macroscopic variation (from specimen to specimen) as well as the microscopic variation (along the crack path in a single specimen). This randomness may be most apparent and most significant for microcracks, when crack-microstructure interactions are also most significant. Microcrack growth rate data are often characterized by a particularly great amount of variability, especially in comparison to growth rate data for large cracks outside of the near-threshold region. Because of this large variability, simple deterministic schemes to compute microcrack-dominated life are often not satisfactory. Algorithms based on best estimates such as mean values cannot account for the significant possibility

of nonconservatively faster growth, and attempts to "envelope" the data with upper bound crack growth curves may be excessively conservative under some conditions (leading to unnecessary rejection of safe hardware).

Thus, microcrack growth is a particularly good candidate for probabilistic methodologies. Unfortunately, microcrack growth also presents special obstacles to developing probabilistic models. In particular, it is often difficult to collect raw fatigue crack growth data of sufficient quality and quantity to compute necessary probabilistic parameters. Crack length measurement is expensive and often cumbersome for microcracks, involving indirect means such as multi-step replication (rather than direct visual inspection of the specimen surface). Microcrack initiation and growth is especially unpredictable, and so it is nearly impossible to obtain data at fixed crack lengths or fixed growth intervals. Smooth specimens are characterized by multiple microcrack initiation and growth, so it is not usually possible to identify *a priori* a single dominant crack, and different microcracks may interact or link up later in life. These difficulties are not insurmountable, but they do influence the path to a solution.

Complete solution of the probabilistic, microstructure-based fatigue life prediction problem requires two steps. First, we must select an appropriate stochastic fatigue crack growth model to explain reasonably the macroscopic variation (from different tests) as well as the microscopic variation (along the crack path in each test) in the material test data. Second, we must select a robust, efficient, and accurate probabilistic method for integrating the stochastic fatigue crack growth model to predict the life.

The selected stochastic fatigue crack growth (SFCG) model should be as simple as possible while maintaining a reasonable accuracy for the prediction of the fatigue crack growth damage accumulation. The model of Ortiz [1] had been an intriguing SFCG option in our original program planning, because it attempts to address the influence of microstructure on rate variation along the crack path. This model uses a random fatigue crack growth (FCG) model to deal with the macroscopic variation, and an additional stochastic process for the FCG model to deal with the microscopic variation. Unfortunately, the Ortiz model proved to be incompatible with the quantity and quality of microcrack data which could be generated under the given experimental conditions, as discussed above. Several other advanced stochastic fatigue growth models also share the same fundamental limitation, including the Markov and semi-Markov chain models as proposed by Bogdanoff and others.

Our current approach is to work with the lognormal random variable model proposed by Yang *et al.* [2], which avoids these difficulties. The simplest form of the lognormal random variable model assumes the random process has a correlation time of infinity, so the correlation parameter for the crack growth rate does not have to be calculated. As a result, all the statistics required for this model can be estimated from a limited amount of test data, which is particularly attractive for real engineering problems. Furthermore, with this simple model, it is relatively easy to predict life with available probabilistic methods. This model is also flexible enough to permit us to consider the possibility of a non-infinite correlation time (or correlation distance, like the Ortiz model) later in our investigations, without necessarily having to perform computations on a large data base.

---

1. K. Ortiz and A. Kiremidjian, *Engineering Fracture Mechanics*, Vol. 29, 1988, pp. 317-334.

2. J. N. Yang, W. H. Hsi, and S. D. Manning, "Stochastic Crack Propagation with Applications to Durability and Damage Tolerance Analyses," AFWAL-TR-85-3062, Air Force Wright Aeronautical Laboratories, 1985.

This lognormal random variable model is composed of a random FCG law and a stochastic process which can be denoted as follows:

$$\frac{da}{dN} = f(\Delta K, a, R)Z(t)$$

where da/dN is the crack growth rate, $f(\Delta K, a, R)$ is a user-defined function (FCG model) of stress intensity factor range, ΔK, crack size, a, stress ratio, R, and perhaps other variables, including microstructural features, and $Z(t)$ is a lognormal random variable which is used to account for all the random variabilities at any time, t (expressed in terms of the number of cycles, N).

These investigations are actively in progress at this writing, so it is not possible to show detailed computations or complete results. One example of the SFCG model in application to a particular data set is shown in Figure 1. Here the lines describing the 1%, 50% (mean value), and 99% probability of exceedance in growth rate as computed from the SCFG model are superimposed on the raw crack growth data from Specimen #347 (see First Annual Report for test details), with a simple Paris Law as the user-selected FCG model. Further details about the structure of the model, the computational approach, and the results will be presented in later progress reports.

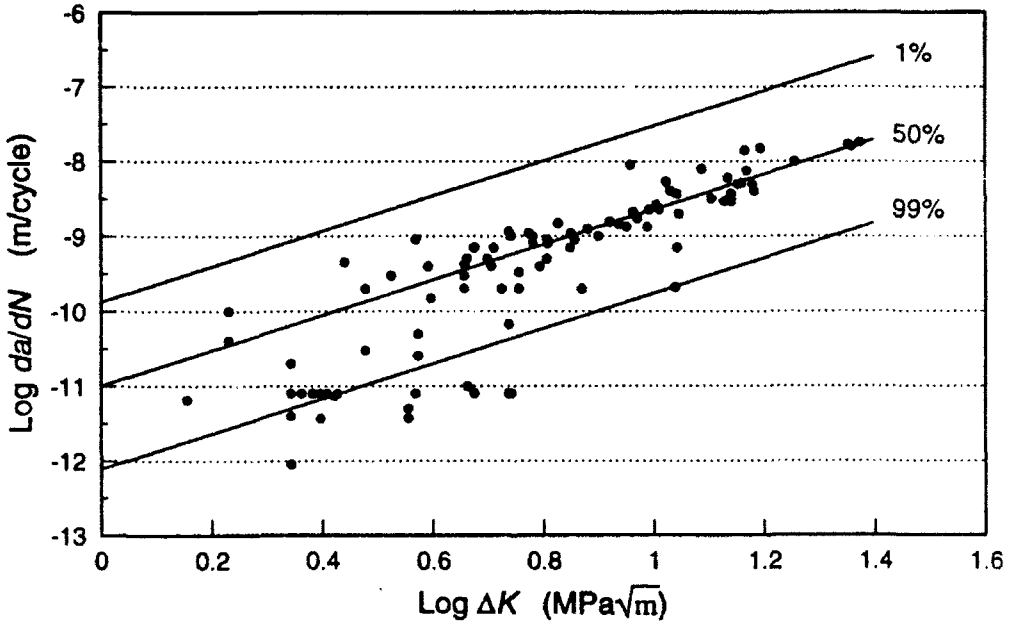

Figure 1. Illustration of the stochastic FCG model with data from specimen #347

Future Work

Our immediate priorities are to resolve the large crack vs. microcrack issue and to continue development of the stochastic crack growth models. The stochastic modeling efforts will begin to merge with the microstructural modeling in a process which has at least two goals: first, to determine if microstructural variability plays a significant role in overall crack growth rate variability, and second, to develop meaningful fatigue damage relationships which can be integrated to generate probabilistic descriptions of total S-N fatigue life.

SCALING LAWS FOR FATIGUE CRACK GROWTH OF LARGE CRACKS IN STEELS

K. S. CHAN

SOUTHWEST RESEARCH INSTITUTE

MATERIALS AND MECHANICS DEPARTMENT

P.O. DRAWER 28510

SAN ANTONIO, TEXAS 78228-0510

ABSTRACT

A set of scaling laws has been developed for describing intermittent as well as continuous fatigue crack growth of large cracks in steels in the power-law regime. The proposed scaling laws are developed on the basis that fatigue crack growth occurs as the result of low-cycle fatigue failure of a crack-tip element whose width and height correspond to the dislocation cell size and barrier spacing, respectively. The results show that the effects of microstructure on fatigue crack growth can be described entirely in terms of a dimensionless microstructural parameter, ξ, which is defined in terms of yield stress, fatigue ductility, dislocation cell size, and dislocation barrier spacing. For both discontinuous and continuum crack growth, the crack extension rate, da/dN, scales with ξ and $\Delta K/E$, where ΔK is the stress intensity range and E is Young's modulus. Application of the model to HSLA and conventional ferritic, ferritic/pearlitic, and martensitic steels reveals that the lack of a strong microstructural influence on fatigue crack growth in the power-law regime is due to increasing yield stress and fatigue ductility with decreasing dislocation barrier spacing, which leads to a narrow range of ξ values and crack growth rates. Variation of da/dN data with microstructure in HSLA-80 steels is explained in terms of the proposed model. Other implications of the scaling laws are also presented and discussed in conjunction with several fatigue models in the literature.

INTRODUCTION

Fatigue crack growth of large cracks in metals and alloys can generally be divided into three characteristic regimes [1]: (1) a near-threshold regime where the growth response is sensitive to microstructure, (2) a power-law regime where microstructure has little effect on the propagation rate, and (3) a rapid growth regime that is dominated by quasi-static crack extension, and fracture toughness (e.g., the K_{IC} value), and is sensitive to microstructure. As shown in Figure 1, the power-law may be subdivided into intermittent and continuous growth regimes. For many alloys, there are considerable overlaps between the intermittent and continuous growth regimes that they become undistinguishable and appear as a single power-law regime. Excellent reviews of the effects of microstructure on fatigue crack growth have been presented by Ritchie [1], Suresh [2], Davidson and Lankford [3], as well as by others [4].

While the lack of microstructural influence in the Paris (power-law growth) regime [5] is well-recognized, its existence is poorly understood. The conventional explanation for microstructure-insensitive fatigue crack growth is that the cyclic plastic zone size is larger than a characteristic microstructural unit size and behaves in a continuum manner. As a result, crack growth is dominated by the cyclic crack-tip opening displacement and occurs on every cycle (continuous or continuum growth). One possible criticism of this explanation is that continuum growth theories [6-8] predict an inverse relationship between fatigue crack growth rate and yield stress. Since the yield stress depends on microstructure, one would think the fatigue crack growth rate should at least mildly depend on microstructure. Yet, numerous studies [10-13] have shown that the fatigue crack growth rates of a large number of metals [13], including steels [10-12], Al- [11], and Ti-alloys [10-11] correlate with the elastic modulus only in the continuum growth regime. On the other hand, compilation of fatigue crack growth data for steels of various yield stresses shows a wide scatter band and not a single curve [14], suggesting that the yield strength, if not the microstructure, might be of some importance.

Recent work has revealed that fatigue crack growth does not occur on a cycle-by-cycle basis in the lower ΔK end of the power-law regime [3,15-17]. Instead, crack growth proceeds intermittently with periodic arrests and waiting periods between individual growth increments (intermittent growth). The incremental growth distance, as determined by the striation spacing, is relatively constant and ranges from 0.1 to 0.3 μm, which is on the order of the dislocation cell size [3,17]. The intermittent growth process is generally modeled by considering that the crack-tip process zone behaves like a low-cycle fatigue (LCF) specimen [17-26]. During strain cycling, the crack-tip LCF element accumulates fatigue damage and fails in accordance to the Coffin-Manson law. The intermittent growth models predict that fatigue crack growth is discontinuous, and the corresponding rate is sensitive to the size of the crack-tip LCF element, which is generally related to a characteristic microstructural length.

The conflicting views about the role of microstructure in fatigue crack growth in the power-law regime bear important consideration in Cu-containing high-strength low-alloy (HSLA) steels such as HSLA-80 [27] (or A710, Grade A, Class 3 in ASTM designation [28]). This class of steels derives its high strength from a combination of a fine grain size (1-2 μm) and precipitation hardening by fine ε-Cu precipitates on the order of 5-20 nm in diameter [29,33]. Fatigue crack growth characterization of HSLA-80 and A710 steels showed a large scatter band with a 5X variation in crack growth rates at a given K level [27]. Transmission electron microscopy has revealed that the higher crack growth rate corresponds to a steel (FZZ) containing Cu precipitates with an average diameter of 6.6 nm, while the lower crack growth rate corresponds to a steel (GAH) with 17.5 nm Cu-precipitates, as shown in Figure 2 [33]. The observation suggests that the size or mean free path of Cu-precipitates might be a factor in determinating the fatigue crack growth response of this class of HSLA steels.

The objective of this article is to present the results of an investigation whose goal was to develop scaling laws for describing the fatigue crack growth behavior of Cu-bearing HSLA steels. The impetus of the modeling effort was the lack of understanding on the effects of microstructural size scale on fatigue crack growth of large cracks in the power-law regime. In this paper, fatigue crack growth laws will be reviewed to highlight the current understanding of the role of microstructure in the power-law growth regime. A generalized model that relates the crack growth kinetics of large cracks directly to relevant microstructural size parameters will be presented. Application of the model to HSLA-80 steels will then be illustrated. Finally, the validity of the model will be tested against experimental results of ferritic, ferritic/pearlitic, bainitic, and martensitic steels in the literature. The purpose of the comparison is two-fold: (1) to test the range of applicability of the model, and (2) to provide possible explanations for the apparent lack of microstrutural influence on fatigue crack growth of large cracks in steels. The use of two normalized parameters for scaling the fatigue crack growth rate of large cracks in steels will be demonstrated in the power-law regime.

REVIEW OF FATIGUE CRACK GROWTH LAWS

Numerous fatigue crack growth laws have been proposed over the last thirty years. Formulated in terms of linear-elastic fracture mechanics, these crack growth laws relate the incremental crack extension per fatigue cycle, da/dN, to the stress intensity range, ΔK. The most well-known fatigue crack growth law is the Paris power-law relation given by [5]

$$\frac{da}{dN} = C\Delta K^m \qquad (1)$$

where C and m are empirical constants. Modifications of the Paris equation to treat stress ratio effect or the presence of a growth threshold are also available in the literature. Most of these models are empirical and provide little information about the effects of microstructural size scale on the crack growth kinetics.

Fatigue crack growth occurs during every cycle at high ΔK. In this continuum growth regime, the crack growth rate, which is in the range of 10^{-6} to 10^{-3} m/cycle, is dominated by the cyclic crack-tip opening displacement, $\Delta CTOD$. For this reason, continuum growth models are generally based on the assumption that the incremental growth distance per cycle is one unit [7], or a fraction, of the $\Delta CTOD$ [34]; thus,

$$\frac{da}{dN} = C_1 \Delta CTOD \tag{2}$$

where C_1 is usually taken to be 0.5 [34]. For small-scale yielding [7],

$$\Delta CTOD = \frac{\Delta K^2}{4\sigma_y E} \tag{3}$$

leading to [7]

$$\Delta CTOD = \frac{C_1 \Delta K^2}{4\sigma_y E} \tag{4}$$

when Eq. (2) and (3) are combined. Eq. (4) indicates that the crack growth rate scales with $\Delta K^2/(\sigma_y E)$ where E is Young's modulus and σ_y is yield stress. Comparison of model with experimental results indicated that Eq. (4) generally overpredicts the fatigue crack growth rate, meaning that the value for C_1 should be less than 0.5. Furthermore, the experimental crack growth rates have been found to correlate with $(\Delta K/E)^2$, specifically, empirical relations of the form [10-12]

$$\frac{da}{dN} = C_2\left[\frac{\Delta K}{E}\right]^2 \tag{5}$$

where C_2 is a fitting parameter. Reported values of C_2 are ≈ 3 [10], 5.4 [11], and 8 [12]. Like Eq. (1), Eqs. (4) and (5) provide no insight on the role of microstructural scale in continuum fatigue crack growth. In fact, Eq. (5) implies that microstructure plays no role in the continuum growth regime. Theoretical models of Frost, et al. [35], and Weertman [36], which relate the fatigue crack growth rate to the blunting of the crack tip whose radius is dictated by the surface energy, are in the form as given by Eq. (5). The values of C_2 were predicted to be ≈ 3 [5,36].

It is well-recognized that fatigue crack growth in the intermediate ΔK range occurs intermittently [3]. Early models of the discontinuous fatigue growth behavior were developed based on the assumption that fatigue damage accumulated at every cycle. Crack extension occurred when the accumulated fatigue damage reached a critical value [7,8,34,37]. Proposed measures of fatigue damage included the cumulative hysteresis energy [7], ΔCTOD [8,37], and plastic strain range [34]. Both the cumulative hysteresis energy and ΔCTOD criteria led to [7,8,37]

$$\frac{da}{dN} = \frac{C_3\Delta K^4}{\sigma_y^2 E U} \tag{6}$$

where C_3 is a numerical constant, and U is the total absorbed hysteresis energy per newly created surface area. A significant difference between continuum and discontinuous crack growth is in the increase of the crack growth exponent, m, from 2 to 4.

McClintock [34] was the first person to introduce the concept of a "structural size" over which accumulation of cyclic plastic strain occurred. By applying the Coffin-Manson law to a

microstructural element located at a characteristic distance, l, ahead of the crack tip. McClintock showed that accumulation of cyclic plastic strain within the structural element during fatigue would lead to intermittent crack growth with the average rate described by [34]

$$\frac{da}{dN} = \frac{C_4}{l}\left[\frac{\varepsilon_y}{\varepsilon_f'}\right]^2\left[\frac{\Delta K}{\sigma_y}\right]^4 \tag{7}$$

where ε_y and ε_f' are the yield strain and fatigue ductility, respectively. Subsequent crack growth models developed based on the concept of a microstructural unit size where the damage criterion is applied include those by Antolovich and co-workers [21,22], Kujawski and Ellyin [24], Mazumder [25], and Lanteigue and Bailon [20]. In the models of Majumdar and Morrow [18], Chakrabortty [19], and Starke, et al. [26], a series of LCF specimens was considered to lie at various distance within the cyclic plastic zone ahead of the crack tip. The crack growth laws were then developed by treating failure of individual LCF specimens in terms of the linear fatigue damage rule.

In Davidson's fatigue crack growth model [23], fatigue damage was envisioned to commence when slip, initiated from the crack tip, was blocked by obstacles located ahead of the crack tip. The obstacle spacing, or slip blockage distance, was then considered the unit size of the microstructural element whose failure would lead to an incremental crack growth. As in other models [21-26], failure of the crack-tip microstructural element was treated via the Coffin-Manson law. Unlike other models, the crack extension distance was considered to be different from the slip distance. This view of the fatigue crack growth process is similar to that subsequently employed by Roven and Nes [17] to develop their fatigue model. While conceptually similar, the Roven and Nes model [17] is considerably simpler and contains fewer empirical constants than Davidson's model [23]. The former crack growth model is used heavily in this investigation, and will be described in detail in the next section.

A MICROSTRUCTURE-BASED FATIGUE CRACK GROWTH MODEL

The model of Roven and Nes [17] considers the LCF failure of a crack-tip element of width s and height d, where s and d are striation and dislocation barrier spacing, respectively, as shown schematically in Figure 3. Figure 3(a) shows that the crack-tip element is embedded in the cyclic plastic zone, while Figure 3(b) illustrates the LCF failure process of the crack-tip element by irreversible motion of dislocations between the dislocation barriers. The selection of striation spacing as the width of the crack-tip element was motivated by the observation that discontinuous fatigue crack growth in iron and low-carbon steels is characterized by a constant striation spacing in the range of 0.1 - 0.3 μm [17]. Additionally, the striation spacing appears to correlate with either dislocation cell size or wall spacing, which are also on the order of 0.1 - 0.3 μm [17]. This implies that the incremental crack growth distance (striation spacing) corresponds to failure of a dislocation cell-element. On this basis, the fatigue crack growth rate associated with LCF failure of a crack-tip element is given by [17,23]

$$\frac{da}{dN} = \frac{s}{N_s} \tag{8}$$

where N_s is the number of fatigue cycle required to cause the observed crack extension (striation spacing), s.

Fatigue failure of the crack-tip element is considered to be governed by the Coffin-Manson law described by [38,39]

$$\frac{\Delta\varepsilon^p}{2} = \varepsilon_f'(2N_s)^{-b} \tag{9}$$

where $\Delta\varepsilon^p$ is the plastic strain range and b is the fatigue ductility exponent. Note that Eq. (9) is written such that b is positive, while fatigue ductility is generally given as a negative quantity in the literature [40,41]. The cyclic crack-tip opening displacement and plastic strain range can be related to the dislocation barrier spacing, d, according to

$$\Delta\varepsilon_{tip}^{p} = \frac{\Delta CTOD}{d} \tag{10}$$

with ΔCTOD given by Eq. (3). Substituting Eqs. (3) and (10) into Eq. (9) leads to

$$\frac{1}{N_s} = \left[\frac{1}{4}\left(\frac{1}{2^{1-b}\sigma_{ys}\varepsilon_f' d}\right)\left(\frac{\Delta K^2}{E}\right)\right]^{1/b} \tag{11}$$

which gives

$$\frac{da}{dN} = \xi^{1/b}(2s)^{1-1/b}\left[\frac{\Delta K}{E}\right]^{2/b} \tag{12}$$

with

$$\xi = \frac{Es}{4\sigma_y\varepsilon_f' d} \tag{13}$$

when Eq. (11) is substituted into Eq. (8).

Eq. (12) is a general expression for discontinuous fatigue crack growth and has the form as the Paris power-law with m = 2/b and C being a function of E, s, and the dimensionless parameter, ξ, which contains all of the microstructure-dependent parameters (σ_y, ε_f', d, and s). For the special case of b = 0.5 in the Coffin-Manson law, Eq. (12) becomes

$$\frac{da}{dN} = \frac{\xi^2}{2s}\left[\frac{\Delta K}{E}\right]^4 \tag{14}$$

which is somewhat similar to Eq. (6) due to Rice [7], Weertman [8], and Mura [37].

For continuum crack growth, b = 1 and crack extension occurs at every cycle. Eq. (12) is reduced to

$$\frac{da}{dN} = \xi\left[\frac{\Delta K}{E}\right]^2 \tag{15}$$

which can be re-expressed as

$$\frac{da}{dN} = \phi \Delta CTOD \tag{16}$$

with

$$\phi = \frac{s}{\varepsilon_f' d} \tag{17}$$

and ΔCTOD given by Eq. (3). Note that Eq. (15) is identical to Eq. (5), which is based on experimental observations, while Eq. (16) is identical to Eq. (2), which is based on a continuum formulation. The potential advantage of Eqs. (12), (15), and (16) over Eqs. (2) and (5) is that they provide additional information about the role of microstructure-related parameters including yield stress (σ_y), fatigue ductility (ε_f'), dislocation cell size (s), and dislocation barrier spacing (d) in determining the crack growth rate.

Crack closure or a growth threshold, ΔK_{TH}, can be incorporated into the proposed model by recognizing the fact that these two related phenomena only affect the driving force for crack growth.

and they have no effect on intrinsic fatigue properties of a particular microstructure, which the microstructural parameter, ξ, signifies. Incorporating the proposed model to include crack closure or a growth threshold can be accomplished by replacing the stress intensity range, ΔK, in Eqs. (3), (11), (12), (14), and (15) with an effective stress intensity range, ΔK_{eff}, given by [3]

$$\Delta K_{eff} = \Delta K - \Delta K_{cl} \tag{18}$$

or

$$\Delta K_{eff} = \Delta K - \Delta K_{th} \tag{19}$$

where ΔK_{cl} is the stress intensity range due to crack closure, and ΔK_{TH} is the growth threshold. The remainder of this article will evaluate various implications of the proposed model against experimental data of steels with a variety of microstructures.

APPLICATION OF THE FATIGUE MODEL TO STEELS

The microstructure-based fatigue model has been applied to elucidate the possible influence of microstructure on the fatigue crack growth behavior of HSLA steels [27,29,40-43] and conventional ferritic [44], ferritic/pearlitic [45-50], bainitic [11], and martensitic steels. Specifically, the fatigue model has been exercised to obtain the crack growth curves for steels with various microstructures, and the calculated curves are compared against experimental results in the literature. The evaluation is limited to the power-law growth regime only, as the effects of microstructure on the near-threshold or threshold of steels are well-established [1,3,55].

Material inputs to the fatigue model include the yield stress (σ_y), fatigue ductility (ε_f'), fatigue ductility exponent (b), and the dislocation barrier spacing (d). When available, reported results of these parameters were used. Otherwise, estimates or measurements of these parameters were made. In most cases, the value of b was obtained from the slope of the da/dN vs ΔK curve in a log-log

plot. Recall that m = 2/b. Reported values of static yield stress were used in all cases. Static yield stress was used rather than the cyclic yield stress because the former is reported more frequently. Microstructural information was not always reported. Under this circumstance, the barrier spacing was measured from published micrographs when available or estimated based on steels with similar strength and microstructure. If none was available, the barrier spacing was estimated based on the yield strength using the relations of yield strength and mean free path established by Gurland [56]. Reported values of ε_f' were generally used. When not available, ε_f' was taken to be the reduction-in-area. In some cases, value of ε_f' for similar steels with equivalent strength and microstructure was used. Values of ε_f' compiled by Hertzberg [57] and Boardman [58] were utilized. When no information was available or poor agreement was obtained between model and experiment, the value of ε_f' was adjusted to fit the model to the experimental curve. The rationale here was that the value of ε_f' for the crack-tip element of the size s x d could be different from that of a conventional LCF specimen of a larger size. The dislocation cell size, s, was taken to be 0.1 μm in most cases, but s = 0.2 μm [17] was also used for ferritic/pearlitic steels. The value of Young's modulus, E, was taken to be 2×10^5 MPa for all steels. A summary of the microstructural parameters is presented in Table I.

Critical experiments were also performed on HSLA-80 steels to verify model calculation. The critical experiments included characterization of striation spacing as a function of stress intensity range and characterization of mean free path of ε-Cu precipitates in HSLA-80 steels. The HSLA-80 crack growth data utilized in the study were originally obtained at the Naval Air War Center (NAWC) and Lehigh University. Some of the test specimens were obtained from these two sources for the characterization tests. Using scanning electron microscopy, fatigue striation spacings were characterized on compact-tension fatigue crack growth specimens from Lehigh University. Transmission electron microscopy was performed on the FZZ and GAH specimens of HSLA-80 supplied by NAWC to determine the size, volume fraction, and mean free path of ε-Cu precipitates. Details of the experimental procedures are described elsewhere [33].

(A) HSLA Steels

The calculated fatigue fatigue crack growth curve for HSLA-80 steel is compared with experimental data [43] in Figure 4. In the model calculation, both the intermittent growth model (Eq. 14) and the continuum growth model (Eq. 15) were used to compute the respective crack growth rates at a given ΔK level. The minimum of these two crack growth rates was taken to be the appropriate da/dN for that ΔK level. In all cases, intermittent growth was dominated by the lower ΔK regime, while continuum growth dominated at high ΔK levels, resulting in a change in slopes in the calculated curve shown in Figure 4. The experimental data included crack growth at stress ratios of R = 0.1 and 0.8, where R is the ratio of minimum stress to maximum stress during a fatigue cycle. Note the absence of a marked R ratio effect in the experimental data, which suggests crack closure is minimal in this data set. The calculated curve is in good agreement with the experimental data for both R = 0.1 and R = 0.8. Both the calculated and observed crack growth curves are bi-linear. The slope of the lower ΔK curve is 4, while it is 2 in the high ΔK regime. This result suggests that intermittent growth occurs at low ΔK while continuum growth dominates at high ΔK. Additionally, the relevant microstructural feature in HSLA-80 steels appears to be the mean free path of the ε-Cu precipitates.

Fatigue striation measurements indicated that the striation spacing was relatively constant with an average value of ≈ 0.1 - 0.2 μm for ΔK levels less than 33 $MPa\sqrt{m}$, as shown in Figure 5. More importantly, the striation spacing was larger than the calculated and the observed crack growth rates, confirming the contention that intermittent growth dominated in this regime. At ΔK levels above 33 $MPa\sqrt{m}$, the striation spacing was larger and increased with ΔK. Additionally, the striation spacing was approximately equal to the calculated and observed crack growth rates, meaning that crack growth indeed occurred on a cycle-by-cycle basis, extending at increments of one or more cell sizes at each fatigue cycle. Thus, the observed change in slope in the da/dN curve in HSLA-80 steels is indeed the consequence of a transition from an intermittent growth to a continuum growth

process. Furthermore, both the intermittent and continuum growth processes scale with the same microstructural parameter, ξ, even though the power to ξ depends on the nature of the crack growth process.

As indicated earlier, the crack growth data of HSLA-80 steels showed a factor of five among nominally identical, though not necessarily microstructurally identical, specimens [33]. To resolve this difference, crack growth calculations were performed for FZZ, GAH, and FD1LT specimens using their measured properties as input to the fatigue model. The FZZ specimen corresponded to the top of the scatter band of the HSLA-80 crack growth data base, while the GAH and FD1LT were near the bottom of that band. The calculated curves are compared with experimental results in Figure 6, together with their corresponding ξ values. The data of Todd et al. [41], is also included in Figure 6 because the data set contains da/dN results for ΔK less than 10 $MPa\sqrt{m}$. Though not perfect, the good agreement between calculation and experiment nonetheless suggests that the variation in fatigue crack growth rate in HSLA-80 steels originates from variations in yield stress, fatigue ductility, and Cu-precipitate spacing, which form the dimensionless microstructural parameter, ξ, defined according to Eq. (13). In particular, FZZ exhibited a higher crack growth rate and ξ value, while FD1LT and GAH manifested lower crack growth rates and higher ξ values.

Comparison of model calculation and the experimental results of VAN-80 steel [49,50], which is a vanadium-containing HSLA steel containing a fine ferritic/pearlitic microstructure, is shown in Figure 7. It is also an independent comparison because all relevant material properties [50] were measured and reported together with the crack growth data in the original studies [49,50]. The excellent agreement gives credence to the proposed model. Notice that the VAN-80 steel also showed evidence of a transition from intermittent growth to continuum growth at high ΔK levels, supporting the observation made in HSLA-80 steels.

(B) Martensitic Steels

Most of the martensitic steels examined contained tempered martensite. The variation in the relevant microstructural feature was the carbide spacing. One steel with untempered martensite [53] was examined, and the relevant feature was the width of the martensitic laths, as pointed out previously by Yoder, et al. [59]. One bainitic steel [11] was examined. Like steels with tempered martensite, the relevant microstructure for the bainitic steel was carbide spacing. Because of the large number of steels examined, only selected examples will be presented here.

Figure 8 shows comparison of the calculated and measured crack growth curves for HY130 [51] and A514J [52] steels in the continuum growth regime. The ξ value for HY130 is 13.5 compared to 6.2 for A514J. The higher ξ value for the former is due to a higher yield strength and lower values for carbide spacing and fatigue ductility. Comparison of the model calculation and experiment in the intermittent growth regime is presented for HY80 [51] and a quenched and tempered (Q&T) steel [50] in Figure 9. In this case, the microstructural parameters of these two steels are relatively similar, leading to similar ξ values and crack growth curves.

(C) Ferritic/Pearlitic Steels

The relevant microstructural feature for the ferritic or ferritic/pearlitic steels examined appeared to be grain or colony size. Comparison of the calculated and experimental crack growth curves for A36 and A537A, which contain a ferritic microstructure with pearlite, is shown in Figure 10. Both steels show subtle differences in yield strength, grain size, fatigue ductility, and fatigue-ductility exponent. The consequence is minor differences in the ξ value and fatigue crack growth rate, as shown in Figure 10.

Comparison of model calculation and experimental data of 1020 steels heat-treated to three different grain sizes is shown in Figure 11. For these steels, the combination of yield stress, fatigue ductility, and grain size led to similar ξ values and fatigue crack growth rates for all three steels at ΔK levels above the growth threshold, ΔK_{Th}. In an earlier study, Yoder et al. [59], have showed that the growth threshold of a number of steels is given by the expression:

$$\Delta K_{th} = 5.5\sigma_y\sqrt{d} \tag{20}$$

where d is the ferrite grain size in this case. Eq. (20) was used in conjunction with the intermittent growth model to obtain the calculated curves shown in Figure 11.

The 1020 steel data shown in Figure 11 were taken from Taira, et al. [45]. Crack closure was measured for these steels, and da/dN data was also correlated with the effective ΔK, ΔK_{eff}, by Taira, et al. [45], as shown in Figure 12. Application of the intermittent growth model to the closure-corrected crack growth data of 1020 steels required replacing ΔK with ΔK_{eff} and a new value for b. Figure 12. Specifically, b was reduced from 0.571 to 0.543, while the dimensionless microstructure parameter, ξ, remained unchanged. This closure independence provides another support for the contention that ξ is the relevant microstructural parameter for scaling da/dN and $\Delta K/E$.

DISCUSSION

(A) Role of Microstructure in Crack Growth

One of the significant findings of this investigation is that fatigue crack growth rate scales with the dimensionless microstructural parameter, ξ, and $\Delta K/E$ in both the intermittent growth and

continuum growth regimes. Since ξ encompasses all relevant microstructural parameters, one only needs to examine variables contained within ξ that are microstructure-dependent, i.e., yield stress, fatigue ductility, and dislocation barrier spacing, to elucidate the role of microstructure in fatigue crack growth in the power-law regime. Figure 13 shows a log-log plot of yield stress vs. barrier spacing for all the steels examined. Despite the scatter, the yield stress is seen to increase with decreasing dislocation barrier spacing according to the Hall-Petch relation [60,61], i.e.,

$$\sigma_y \propto (d)^{-\frac{1}{2}}. \tag{21}$$

Similarly, a plot of log (ε_f') vs. log (d) in Figure 14 shows increasing fatigue ductility with decreasing barrier spacing according to

$$\varepsilon_f' \propto (d)^{-\frac{1}{2}}. \tag{22}$$

Motivated by these findings, $\sigma_y\varepsilon_f'$ is plotted against d in a log-log plot in Figure 15. The result is a scatter band whose average values are represented by a linear curve with a slope of -1, as shown in Figure 15. Thus, the relationship between $\sigma_y\varepsilon_f'$ and d is given by

$$\sigma_y\varepsilon_f' d = U_d \tag{23}$$

where U_d, the cumulative plastic work per unit area of crack growth, appears to vary among the various steels.

The apparent lack of microstructural influence on fatigue crack growth in the power-law regime can be explained in terms of the results shown in Figures 13-15. Recall that da/dN scales with ξ and $\xi = Es/(4\sigma_y\varepsilon_f'd)$. For steels with a fine microstructure, the value of d is small, but the

values of σ_y and ε_f' are larger. Conversely, d is large for steels with coarse microstructures, but the corresponding values for σ_y and ε_f' are lower. The consequence is that the product of $\sigma_y\varepsilon_f'd$, or U_d, is relatively insensitive to microstructure, leading to small variations in the ξ value, and thus the crack growth rate with microstructure. Since σ_y and ε_f' show considerable scatter when correlated with d (Figures 12 and 13), variations in these parameters lead to a range of ξ values and crack growth rates. Thus, part of the experimentally observed crack growth variations actually originates from the microstructure, as observed in HSLA-80 steels in Figure 6.

The ε_f' value for HSLA-80 steels, which ranges from 0.71 to 0.75, was assumed to have the same value as the reduction-in-area. These assumed values are consistant with $\varepsilon_f' = 0.80$, measured for a Nb-bearing HSLA steel containing a high Nb content [62], but are larger than $\varepsilon_f' = 0.20 - 0.24$ for low-Nb HSLA steels [62]. Some of the ε_f' values (A36, A537, A533B, 1020, and low-carbon steels) were obtained by fitting the model to the crack growth data. Those results are therefore not an independent verification of the model. For the two cast steels, the value of $\varepsilon_f' = 0.20$ were required to obtain good agreement between model and experiment. The reported values for these two cast steels were $\approx 0.35 - 0.40$ [47,48]. As indicated earlier, the discrepancies might be attributed to differences in the size of the crack-tip element and the conventional LCF specimen, or to inadequacies of the model. Overall, the ε_f' value for the steels examined ranges from 0.1 to 1, which is within the experimental range [57,58].

(B) Comparison with Previous Crack Growth Models

As indicated earlier, the microstructure-based model yields a crack growth equation that is identical to the continuum growth model of Rice [7]. The main difference between the two models is that in the microstructure-based model, the dimensionless parameter, ϕ, depends on microstructure-sensitive parameters as defined by Eq. (17), while ϕ is assumed to be 1/2 in the

continuum model. Figure 16 shows that the values of ϕ observed in the steels examined range from 0.02 to 0.3, with ϕ increasing with decreasing values of d/s. Interestingly, the value of ϕ extrapolates to 1/2 at the limit of d/s = 1. Since d relates ΔCTOD to $\Delta\varepsilon_{tip}^{P}$ (Eq. 10), the fatigue crack growth rate is directly related to how the ΔCTOD is accommodated by the cyclic plastic flow within the crack-tip element, whose dimensions correspond to characteristic features of the fatigue microstructure.

One form of the present model (Eq. 15) firmly establishes that the experimental correlation between da/dN and $\Delta K/E$ (Eq. 5) is indeed relevant. In fact, such a correlation applies to both the continuum and intermittent growth regime, as observed experimentally [10-13,63]. Different values of C_2 observed by various investigators [10-13] in the continuum growth regime [10-12] can now be explained in terms of variations in yield stress, fatigue ductility, dislocation barrier spacing, and dislocation cell size, i.e, the fatigue microstructure. Figure 17 shows the values of ξ as a function of the ratio of dislocation barrier spacing to cell size, d/s, with no obvious correlation between the two parameters. Thus, Eq. (23) is essentially valid to the first order. The variations in ξ, which ranges from 4 to 25, arises mainly from different values of U_d and partly from variations in the cell size, s. The models of Frost, et al. [35], and Weertman [36] are of the same form described by Eq. (5), as alluded to earlier. The scaling parameters in these models, however, are a constant approximately equal to 3, which is lower than that observed in most steels.

The parameter U_d is reminiscent of the U term in Eq. (6). However, it should be noted that they are parameters with somewhat different physical meanings. The U_d term represents the cumulative plastic work per unit crack area associated with LCF fracture of a crack-tip element of height, d, and width, s (see Figure 3), while U is generally measured over the length of the plastic zone [64-67]. As a result, the value of U is considerably larger than U_d. The implication is that most of the energy supplied by the external load does not go to producing an incremental crack growth. Instead, most of this expended energy goes to deform materials within the crack-tip plastic zone.

Recent TEM observations revealed that fatigue cycling of iron and steels [17,65,69] led to the formation of dislocation sub-cells at low accumulated plastic strains. The dislocation sub-cells subsequently rearranged to form dislocation wall-like structures [68]. In both cases, the size of the dislocation sub-cells and the spacing between dislocation walls are generally between 0.1 - 0.2 μm [17,68,69]. The effect of continued strain cycling was to refine the dislocation cell structure by increasing the population of dislocation cells and wall spacing that is in the 0.1 - 0.2 μm range. This point is best illustrated in Figure 18, which is prepared based on TEM micrographs of Keller, et. al. [68] showing dislocation structures in the interior of fatigue specimens of a Fe-Si alloy. The dislocation cell size near a crack tip in iron has also been shown by Kitagiri, et al., to be about 0.1 - 0.2 μm [70]. Additionally, the dislocation cell size increases with increasing distance from the crack tip [70]. Taken together, these TEM observations suggest most of the cyclic plastic work, U, is expended into refining the dislocation structure within the crack-tip plastic zone, probably via dislocation mechanisms suggested by Kuhlmann-Wilsdorf and Laird [71,72]. The smallest size that a dislocation cellular element can attain is about s x d, with s ≈ 0.1 - 0.2 μm. Further refining of this element size might be impossible, and attempts to do so would lead to LCF failure of the cellular element, producing an incremental growth of length, s, at an energy expenditure of U_d.

The present model is quite similar to that of Antolovich, et al. [22]. The essential difference between the two models is that the role of the dislocation cell size, s, and dislocation barrier spacing, d, is considered in the former model, while only the dislocation cell size is considered in the latter model. The model of Antolovich, et al. [22], can be expressed in a form similar to Eq. (12), resulting in a scaling parameter that is a function of $E/(\sigma_y \varepsilon_f')$, but is, otherwise, independent of an explicit microstructural length parameter.

The proposed model is conceptually similar to that of Davidson [23] and is essentially identical to that of Roven and Nes [17], with the exception of a factor of 1/4 in the ΔCTOD and ΔK relation, Eq. (17). The model of Roven and Nes is expressed in terms of ΔK_{eff}, while ΔK is used in the

present model. As shown in Figures 10 and 11, the different use of the crack driving force parameter results in a small change in the fatigue ductility exponent, b, and has no effect on the dimensionless ξ parameter that scales da/dN with either ΔK or ΔK_{eff}. The value of b ranges from 0.5 to 0.75 in the intermittent growth regime, compared to the range of 0.39 to 0.77 observed for a wide range of steels [57,58]. Thus, the b values derived from the crack growth data are reasonable. However, for materials such as stainless steels [73] whose crack growth exponent is about 6 to 8, the proposed model would have some difficulties unless b values as low as 0.25 to 0.3 are allowed. It should also be noted that the proposed model is difficult to apply to microstructures whose dislocation barriers are not obvious, for example, ferritic [44] or austenitic steels [73] with very large grain size (> 100 μm) or single-crystal alloys. Under these circumstances, the dislocation barrier spacing, d, is obviously not the grain size, as the cyclic plastic zone is embedded well within a single grain. As a result, another characteristic length, which might well be related to the underlying dislocation structure, should be used for d. It is envisioned that the proposed scaling laws can be readily extended to materials that do not form cellular dislocation structures (e.g., planar slip materials) during fatigue. This can be accomplished by relating the dimensions (s and d) of the crack-tip LCF element to the appropriate microstructural length dimensions. Identification of the proper dislocation barrier spacing and crack extension distance for these materials, however, might not be an easy task.

CONCLUSIONS

1. The effects of microstructure on fatigue crack growth in the power-law regime can be described entirely in terms of a dimensionless microstructure parameter, ξ, defined in terms of yield stress, fatigue ductility, dislocation cell size, and dislocation barrier spacing. For both intermittent and continuum crack growth, the crack extension rate, da/dN, scales with ξ and $\Delta K/E$, where ΔK is the stress intensity range and E is Young's modulus.

2. The lack of a strong microstructural influence on fatigue crack growth in the power-law regime of steels is due to increasing yield stress and fatigue ductility with decreasing dislocation barrier spacing, which results in a narrow range of ξ values and crack growth rates. The value of ξ ranges from 4 to 24 for steels examined.

3. In the continuum growth regime, the crack growth rate is a small fraction of the cyclic crack tip opening displacement. The scaling constant between da/dN and ΔCTOD is a dimensionless microstructural parameter, ϕ, which is the ratio of dislocation cell size to the product of dislocation barrier spacing and fatigue ductility. The value of ϕ ranges from 0.02 to 0.3 for steels examined.

4. Variation of da/dN data among HSLA-80 steel specimens is partly due to variations in the mean free path of ε-Cu precipitates, yield stress, and fatigue ductility among individual specimens.

5. The change in the crack growth exponent from 4 to 2 with increasing ΔK levels in HSLA-80 steels arises from the transition of an intermittent growth mechanism to a continuum growth process. The striation spacing is on the order of the dislocation cell size (0.1 - 0.2 μm) and is relatively constant during intermittent growth. The striation spacing is considerably larger and increases with increasing ΔK during continuum growth.

ACKNOWLEDGEMENTS

This work was supported by the Office of Naval Research through ONR Contract No. N00014-91-C-0214. The encouragement by Program Monitor, Dr. A. K. Vasudevan, is acknowledged. The author is also thankful to Dr. R. J. Dexter, ATLSS Center, Lehigh University, for supplying HSLA-80 data and tested specimens, and to Dr. T. M. Scoonover at NAWC for supplying the GAH and FZZ specimens. Technical assistance by Dr. Y-M Pan (SwRI) with the TEM, and Mr. J. Campbell (SwRI) with SEM is acknowledged. The author is thankful to Drs. D. L. Davidson and R. C. McClung, both at SwRI, for their constructive comments, and to Ms. J. A. McCombs for typing the manuscript.

REFERENCES

1. R. O. Ritchie: *Int. Metals Reviews*, Vol. 24, 1979, pp. 205-230.

2. S. Suresh: *Fatigue of Materials*, Cambridge University Press, London, UK, 1991.

3. D. L. Davidson and J. Lankford: *Int. Metals Reviews*, Vol. 37, 1992, pp. 45-76.

4. *Fatigue and Microstructure*, M. Meshii, ed., ASM, Metals Park, OH, 1979.

5. P. C. Paris and F. Erdogan: *J. Basic Engineering*, Trans. ASME, Series D, Vol. 85, 1963, pp. 528-534.

6. R. W. Lardner: *Phil. Mag.*, Vol. 17, 1968, pp. 71-82.

7. J. R. Rice: in Fatigue Crack Propagation, ASTM STP 415, ASTM, Philadelphia, PA, 1967, pp. 247-311.

8. J. Weertman: in Fatigue and Microstructure, M. Meshii, ed., ASM, Metals Park, OH, 1979, pp. 279-306.

9. P. E. Irving and L. N. McCartney: *Metal Science*, Vol. 11, 1977, pp. 351-361.

10. R. J. Donahue, H. M. Clarke, P. Atanmo, R. Kumble, and A. J. McEvily: *Int. J. Fracture Mech.*, Vol. 8, 1972, pp. 209-219.

11. R. C. Bates and W. G. Clark, Jr.: *Trans. ASM*, Vol. 62, 1969, pp. 380-389.

12. G. T. Hahn, R. G. Hoagland, and A. R. Rosenfield: AF33615-70-C-1630, Battelle Memorial Inst., Columbus, OH, August 1971.

13. M. O. Speidel: in High-Temperature Materials in Gas Turbines, P. R. Sahm and M. O. Speidel, eds., Elsevier Scientific Publishers, Amsterdam, Holland, 1974, pp. 207-251.

14. D. P. Wilhem: in Fatigue Crack Propagation, ASTM STP 415, ASTM, Philadelphia, PA, 1967, pp. 363-383.

15. N. M. Grinberg: *Int. J. Fatigue*, 1984, Vol. 6, pp. 229-242.

16. H. J. Roven, M. A. Langφy, and E. Nes: in Fatigue 87, R. O. Ritchie and E. A. Starke, eds., Engineering Materials Advisory Services, Warley, UK, Vol. 1, 1987, pp. 175-184.

17. H. J. Roven and E. Nes: *Acta Metall. Mater.*, Vol. 39, 1991, pp. 1735-1754.

18. S. Majumdar and J. Morrow: in Fracture Toughness and Slow-Stable Cracking, ASTM STP 559, ASTM, Philadelphia, PA, 1974, pp. 159-182.

19. S. B. Chakrabortty: *Fat. Eng. Mat. & Struct.*, Vol. 2, 1979, pp. 331-344.

20. J. Lanteigne and J-P. Baïlon: *Metall. Trans.*, Vol. 12A, 1981, pp. 459-466.

21. G. R. Chanahi, S. D. Antolovich, and W. W. Gerberich: *Metall. Trans.*, Vol. 3, 1972, pp. 2661-2672.

22. S. D. Antolovich, A. Saxena, and G. R. Chassani: *Eng. Fract. Mech.*, Vol. 7, 1975, pp. 649-652.

23. D. L. Davidson: *Acta Metall.*, Vol. 32, 1984, pp. 707-714.

24. D. Kujawski and F. Ellyin: *Eng. Fract. Mech.*, Vol. 20, 1984, pp. 695-704.

25. P. K. Mazumdar: *Acta Metall.*, Vol. 34, 1986, pp. 2487-2492.

26. E. A. Starke, Jr., F. S. Lin, R. T. Chen, and H. C. Heikkenen: in Fatigue Crack Growth Threshold Concepts, D. L. Davidson and S. Suresh, eds., TMS-AIME, Warrendale, PA, 1984, pp. 43-61.

27. T. W. Montemarano, B. P. Sack, J. P. Gudas, M. G. Vassilaros, and H. H. Vanderveldt: *J. of Ship Production*, Vol. 2, No. 3, 1986, pp. 145-162.

28. ASTM A710/A710M-85a: in 1987 Annual Book of ASTM Standards, Vol. 01.04, 1987, ASTM, Philadelphia, PA, pp. 664.

29. A. D. Wilson, C. R. Roper, Jr., and E. G. Hamburg: SAE Paper 870790, 1988, pp. 2.1127-2.1146.

30. R. J. Jessman and G. J. Murphy: *J. Heat-Treating*, Vol. 3, No. 3, 1984, pp. 228-236.

31. G. R. Speich and T. M. Scoonover: in Processing, Microstructure, and Properties of HSLA Steels, A. J. DeArdo, ed., AIME-TMS, Warrendale, PA, 1988, pp. 265-287.

32. M. T. Miglin, J. P. Hirth, A. R. Rosenfield, and W.A.T. Clark: *Metall. Trans. A.*, Vol. 17A, 1986, pp. 791-798.

33. K. S. Chan, D. L. Davidson, and R. C. McClung: *Microstructure-Based Fatigue Life Prediction Methods for Naval Steel Structures*, First Annual Report, ONR Contract No. N00014-91-C-0214, Southwest Research Institute, San Antonio, TX, July 1992.

34. F. A. McClintock: *Fracture of Solids*, D. C. Drucker and J. J. Gilman, eds., John Wiley, NY, 1963, pp. 65-102.

35. N. E. Frost, K. J. Marsh, and L. P. Pook: *Metal Fatigue*, Clarendon Press, Oxford, 1974, p. 235.

36. J. Weertman: in Mechanics of Fatigue, ASME Applied Mechanics Division, Vol. 47, ASME, NY, 1981, pp. 11-19.

37. T. Mura and C. T. Lin: *Int. J. Fract.*, Vol. 10, 1974, pp. 284-287.

38. L. F. Coffin, Jr.: *Trans. ASME*, Vol. 76, 1954, pp. 931-950.

39. S. S. Manson and M. H. Hirschberg: in Fatigue: An Inter-Disciplinary Approach, Syracus University Press, Syracuse, NY, 1964, pp. 133-178.

40. T. W. Montemarano, R. T. Brenna, T. E. Caton, D. A. Davis, R. L. McGaw, L. J. Roberson, T. M. Scoonover, and R. J. Wong: DTNSRDC TM-28-84-17, David W. Taylor Naval Ship Research and Development Center, 1984.

41. J. A. Todd, P. Li, G. Lin, and V. Ramon: *Scripta Metall.*, Vol. 22, 1988, pp. 745-750.

42. L. R. Link: in Fatigue and Fracture Testing of Weldments, ASTM STP 1058, H. I. McHenry and J. M. Potter, eds., ASTM, Philadelphia, PA, 1990, pp. 16-33.

43. R. J. Dexter: ATLSS Center, Lehigh University, Bethlehem, PA, unpublished research, 1993.

44. T. Yokobori, I. Kawada, and H. Hata: in Reports of Research Institute for Stength and Fracture of Materials, Vol. 9, No. 2., Tohoku University, Sendai, Japan, 1973, pp. 35-64.

45. S. Taira, K. Tanaka, and M. Hoshina: in Fatigue Mechanisms, ASTM STP 675, ASTM, 1979, pp. 135-162.

46. J. M. Barson: Trans ASME, Series B, *J. Engineering for Industry*, Vol. 93, 1971, pp. 1190-1196.

47. R. I. Stephens, J. H. Chung, S. G. Lee, H. W. Lee, A. Fatemi, and C. Vacas-Oleas: in Fatigue at Low Temperatures, ASTM 857, R. I. Stephens, ed., ASTM, Philadelphia, PA, 1985, pp. 140-160.

48. R. I. Stephens: in Fatigue Life: Analysis and Prediction, V. S. Goel, ed., ASM, Metals Park, OH, 1986, pp. 69-77.

49. P. E. Bretz, B. L. Braglia, and R. W. Hertzberg: in Weldments: Physical Metallurgy and Failure Phenomena, Proceedings of the 5th Bolton Landing Conference, R. J. Christoffel, E. F. Nippes, and H. D. Solomon, eds., General Electric Company, Schenectady, NY, 1979, pp. 271-283.

50. R. W. Hertzberg and R. H. Goodenow: in Microalloying 75, Union Carbide Corp., Niagara Falls, NY, 1981, pp. 503-516.

51. J. M. Barsom, E. J. Imhof, and S. T. Rolfe: *Eng. Fract. Mech.*, Vol. 2, 1971, pp. 301-317.

52. M. Parry, H. Nordberg, and R. W. Hertzberg: *Welding Journal*, Vol. 51, No. 2, 1972, pp. 485-490.

53. M. F. Carlson and R. O. Ritchie: *Scripta Metall.*, Vol. 11, No. 12, 1977, pp. 1113-1118.

54. E. J. Imhof and J. M. Barsom: in Progress in Flaw Growth and Fracture Toughness Testing, ASTM STP 536, ASTM, Philadelphia, 1973, pp. 182-205.

55. M. E. Fine and R. O. Ritchie: in Fatigue and Microstructure, M. Meshii, ed., ASM, Metals Park, OH, 1979, pp. 245-278.

56. J. Gurland: in Stereology and Quantitative Metallography, ASTM STP 504, ASTM, Philadelphia, PA, 1972, pp. 108-118.

57. R. W. Hertzberg: *Deformation and Fracture Mechanics of Engineering Materials*, John Wiley & Sons, NY, 1976, pp. 448-451.

58. B. Boardman: in ASM Metals Handbook, Vol. 1, 10th Edition, ASM, Metals Park, OH, 1990, pp. 673-688.

59. G. R. Yoder, L. A. Cooley, and T. W. Crooker: in Fracture Mechanics: Fourteenth Symposium—Vol. I: Theory and Analysis, ASTM STP 791, J. C. Lewis and G. Sines, eds., ASTM, Philadelphia, PA, 1983, pp. I-348-I-365.

60. E. O. Hall: *Proc. Phys. Soc.*, Vol. 64, Section B, 1951, pp. 747-753.

61. M. J. Petch: *J. Iron & Steel Indust.*, Vol. 174, 1953, pp. 25-28.

62. Y. H. Kim and M. E. Fine: *Metall. Trans.*, Vol. 13A, 1982, pp. 59-72.

63. S. Pearson: *Nature*, Vol. 211, 1966, pp. 1077-1078.

64. S. Ikeda, J. Izumi, and M. E. Fine: *Eng. Fract. Mech.*, Vol. 9, 1977, pp. 123-136.

65. P. K. Liaw, M. E. Fine, and D. L. Davidson: *Fat. Eng. Mat. & Struct.*, Vol. 3, 1980, pp. 59-74.

66. P. K. Liaw, S. I. Kwun, and M. E. Fine: *Metall. Trans.*, Vol. 12A, 1981, pp. 49-55.

67. P. K. Liaw: *Eng. Fract. Mech.*, Vol. 22, 1985, pp. 237-245.

68. R. R. Keller, W. Zielinski, and W. W. Gerberich: *Scripta Metall. et Mater.*, Vol. 26, 1992, pp. 1523-1528.

69. W. J. Bartina, M. Aziza, A. C. Rinella, and S. Yue: in HSLA Steels: Metallurgy and Applications, ASM, Metals Park, OH, 1986, pp. 763-770.

70. K. Katagiri, J. Awatani, A. Omura, K. Koyanagi, and T. Shiraishi: in Fatigue Mechanisms, J. T. Fong, ed., ASTM STP 675, ASTM, Philadelphia, PA, 1979, pp. 106-128.

71. D. Kuhlmann-Wilsdorf and C. Laird, *Mater. Sci. & Eng.*, Vol. 27, 1977, pp. 137-156.

72. C. Laird, P. Charsley, and H. Mughrabi: *Mater. Sci. & Eng.*, Vol. 81, 1986, pp. 433-450.

73. A. W. Thompson: *Eng. Fract. Mech.*, Vol. 7, 1975, pp. 61-68.

74. K. D. Challenger, R. B. Brucker, W. M. Elger, and M. J. Sorek: *Welding Research Supplement*, August 1984, pp. 254-5-262-5.

75. M. F. Carlson, B. V. Narasimha Rao, and G. Thomas: *Metall. Trans. A*, Vol. 10A, 1979, pp. 1273-1284.

76. Metals Handbook, Vol. 7, 8th Edition, ASM, Metals Park, OH, 1972.

LIST OF FIGURES

Figure 10. Comparison of calculated and experimental da/dN curves for A36 and A537A steels [46].

Figure 11. Calculated da/dN vs. ΔK curves compared to experimental data of 1020 steels. Experimental data are from Taira, et al. [45].

Figure 12. Calculated da/dN vs. effective ΔK curves compared to experimental data of 1020 steels. Experimental data are from Taira, et al. [45].

Figure 13. Dependence of yield stress on dislocation barrier spacing, d.

Figure 14. Dependence of fatigue ductility on dislocation barrier spacing, d.

Figure 15. Dependence of $\sigma_y \varepsilon_f'$ on dislocation barrier spacing, d.

Figure 16. The lack of dependence of the dimensionless microstructural parameter, $\xi = Es/\sigma_y \varepsilon_f' d$, on the ratio of dislocation barrier spacing to dislocation cell size, d/s.

Figure 17. The dependence of the dimensionless microstructural parameter, $\phi = s/(\varepsilon_f' d)$, on the ratio of dislocation barrier spacing to dislocation cell size, d/s.

Figure 18. Distribution of dislocation cell size showing refinement of cell size with increasing fatigue cycles. Based on results of Keller, et al. [68].

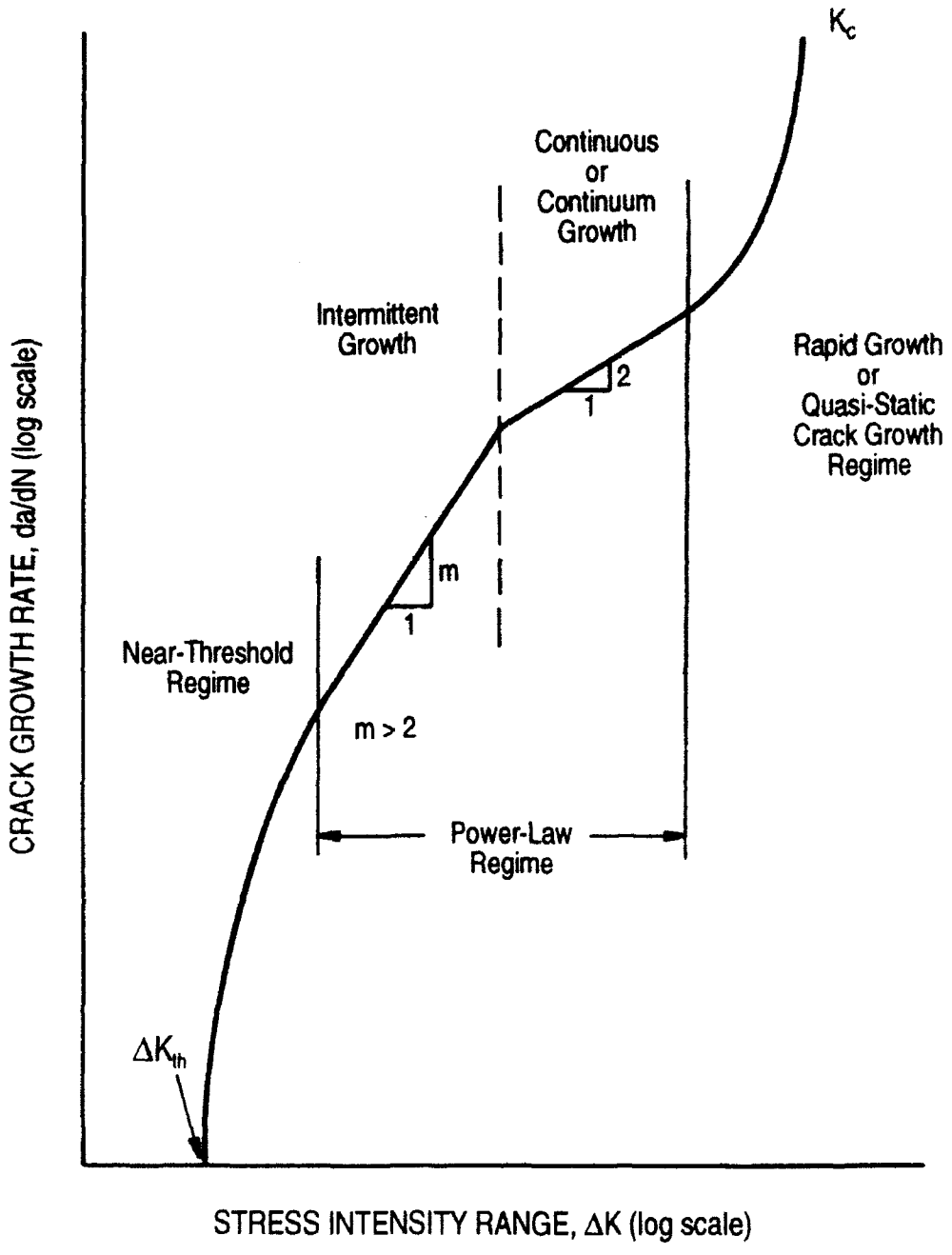

Figure 1. A schematic showing the various growth regimes in a fatigue crack growth curve.

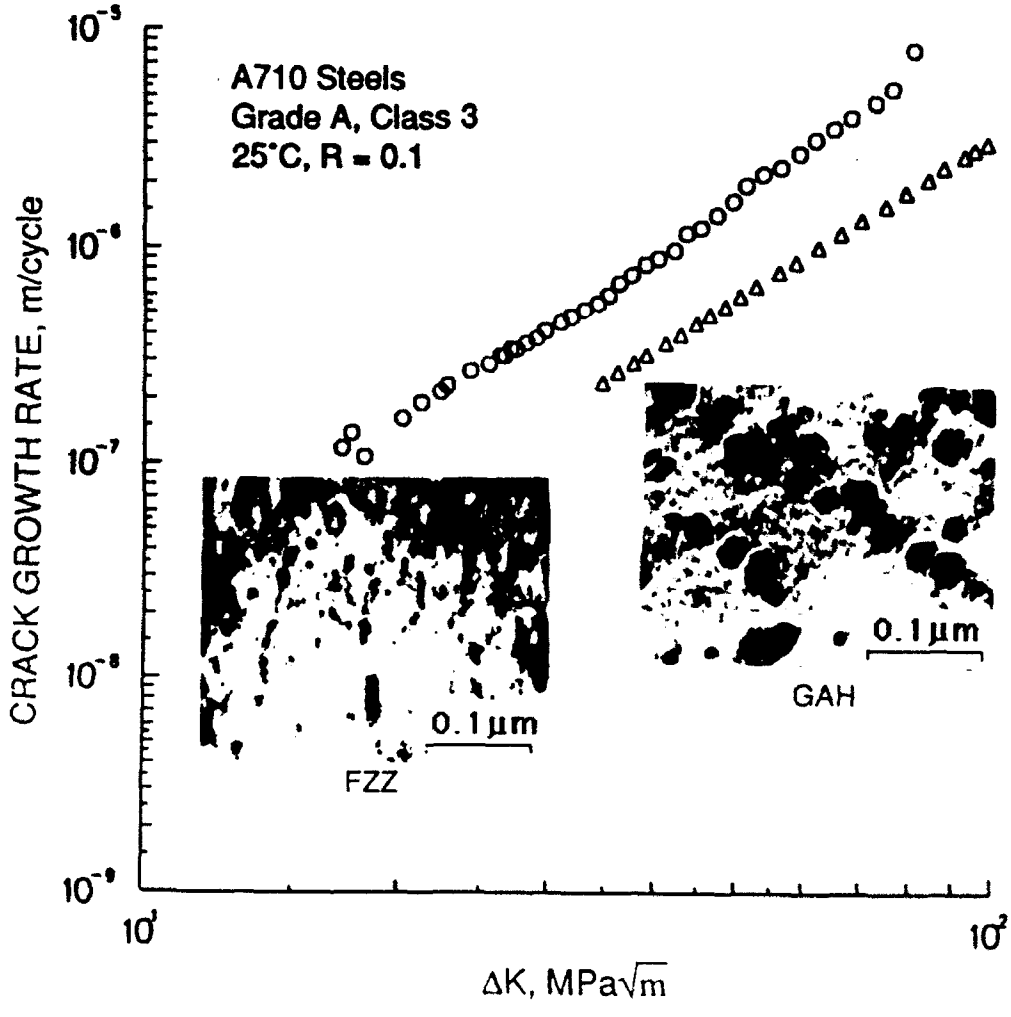

Figure 2. Dependence of fatigue crack growth rate on the size of ε-copper precipitates in FZZ and GAH plates [33].

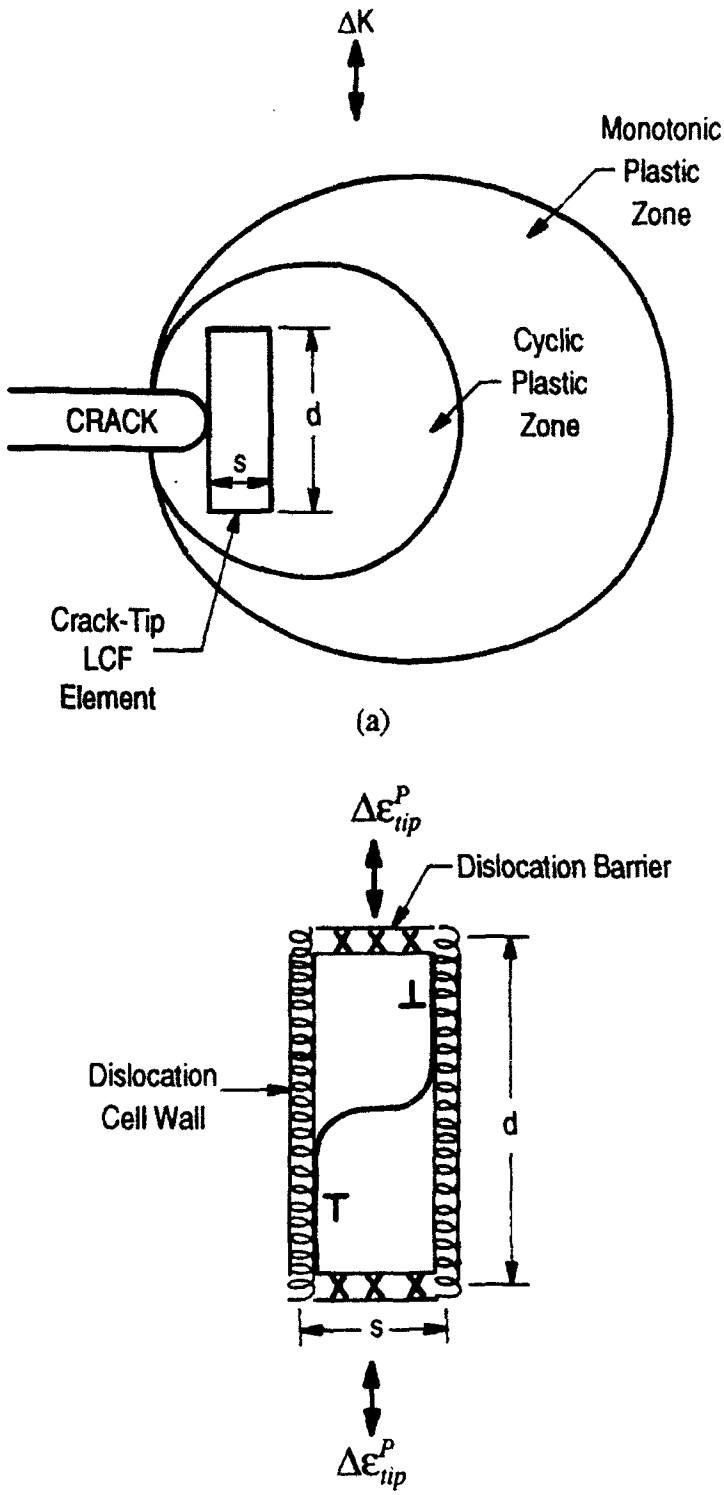

Figure 3. Schematics of the proposed low-cycle fatigue crack-tip element for modeling fatigue crack growth: (a) location of the crack-tip element relative to the cyclic and monotonic plastic zones, and (b) characteristic microstructural lengths of the crack-tip element.

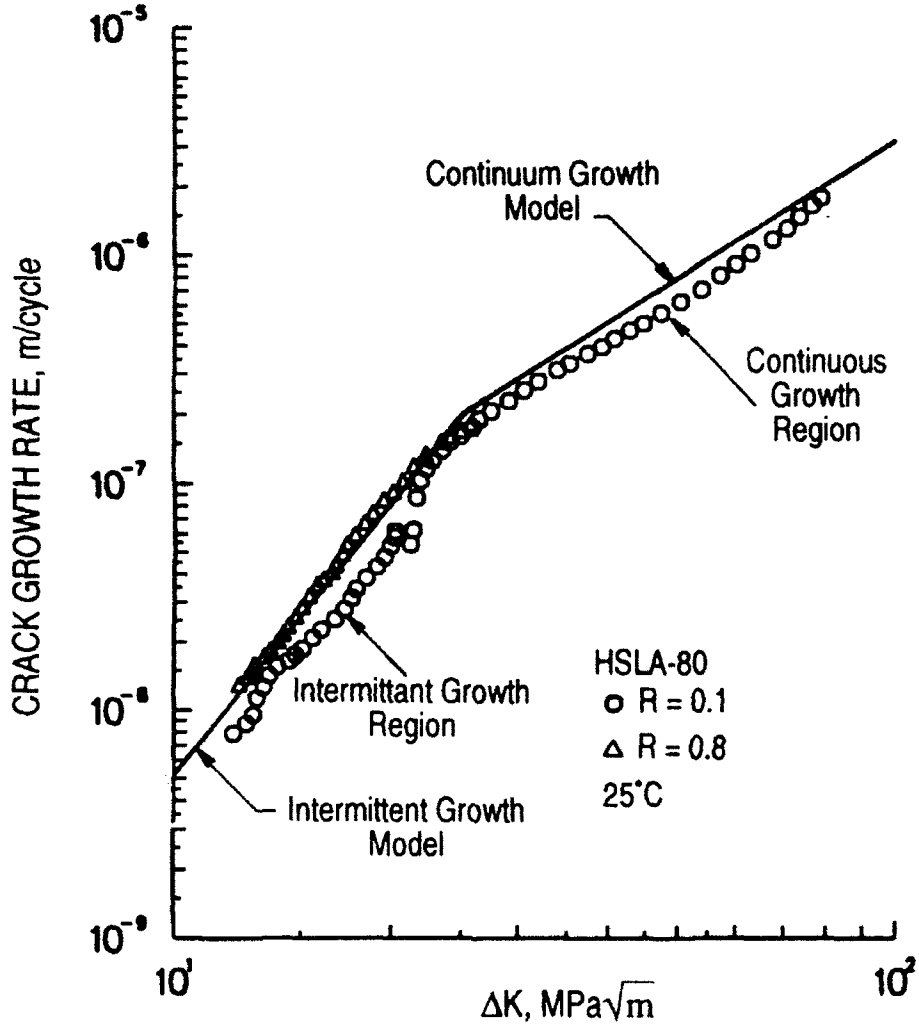

Figure 4. Comparison of experimental and calculated da/dN curves for HSLA-80 steels at R = 0.1 and 0.8. Experimental crack growth data are from R. J. Dexter [43].

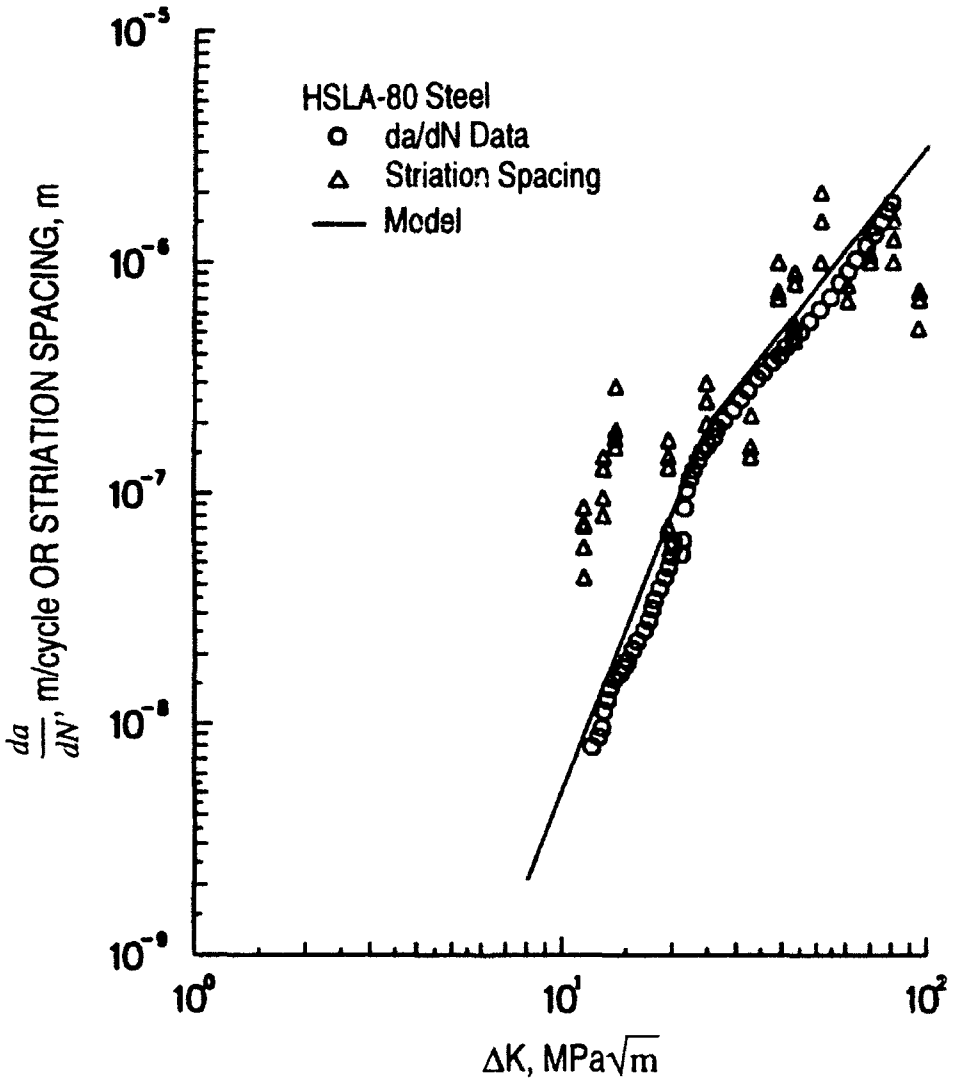

Figure 5. Comparison of experimental and calculated da/dN curves with striation spacings for HSLA-80 steel at R = 0.1. Experimental crack growth data are from R. J. Dexter [43].

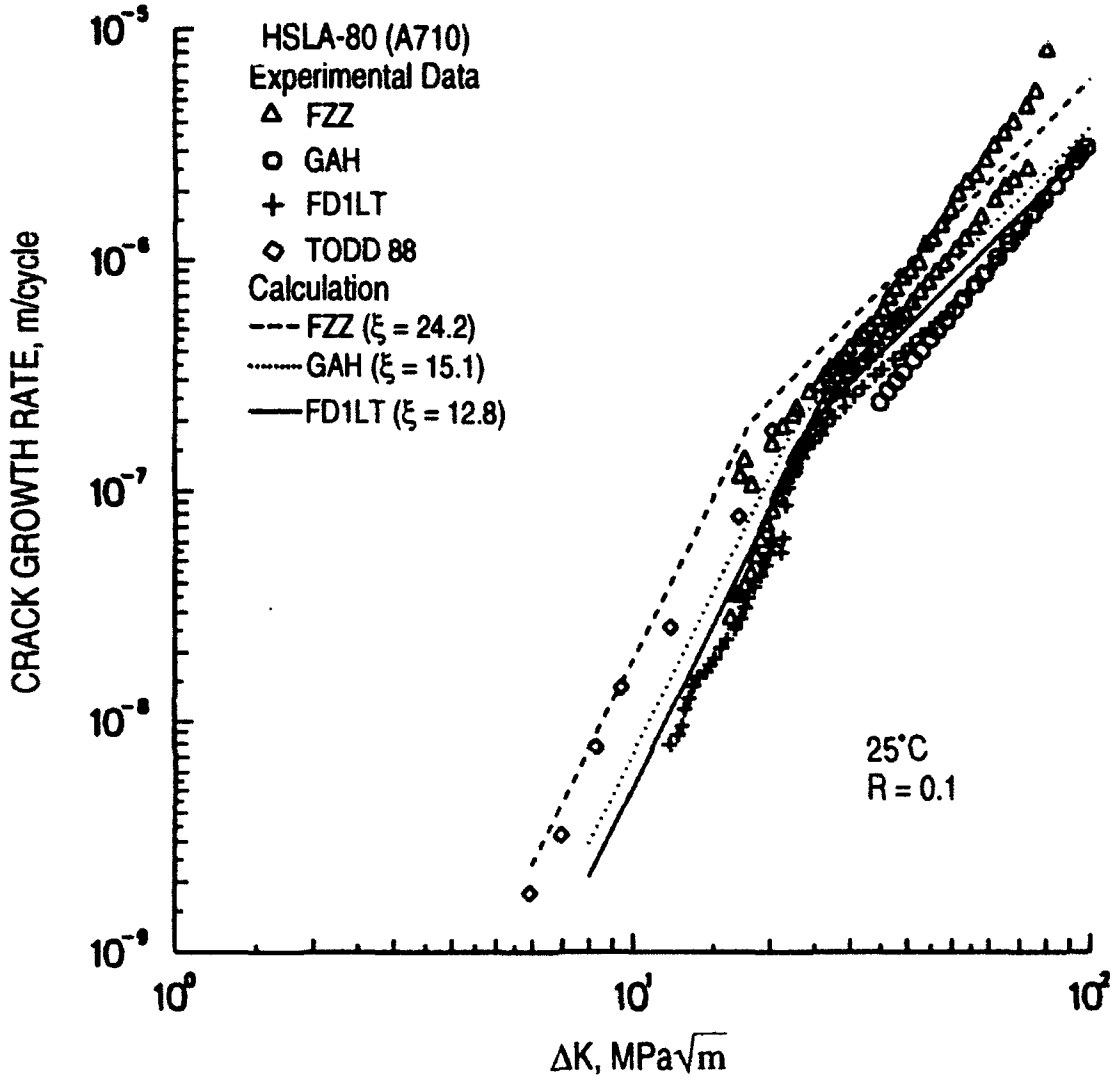

Figure 6. Comparison of experimental and calculated da/dN curves for individual HSLA-80 steel specimens. Experimental data are from R. J. Dexter [43], T. M. Montemarano, et al. [40], and Todd, et al. [41].

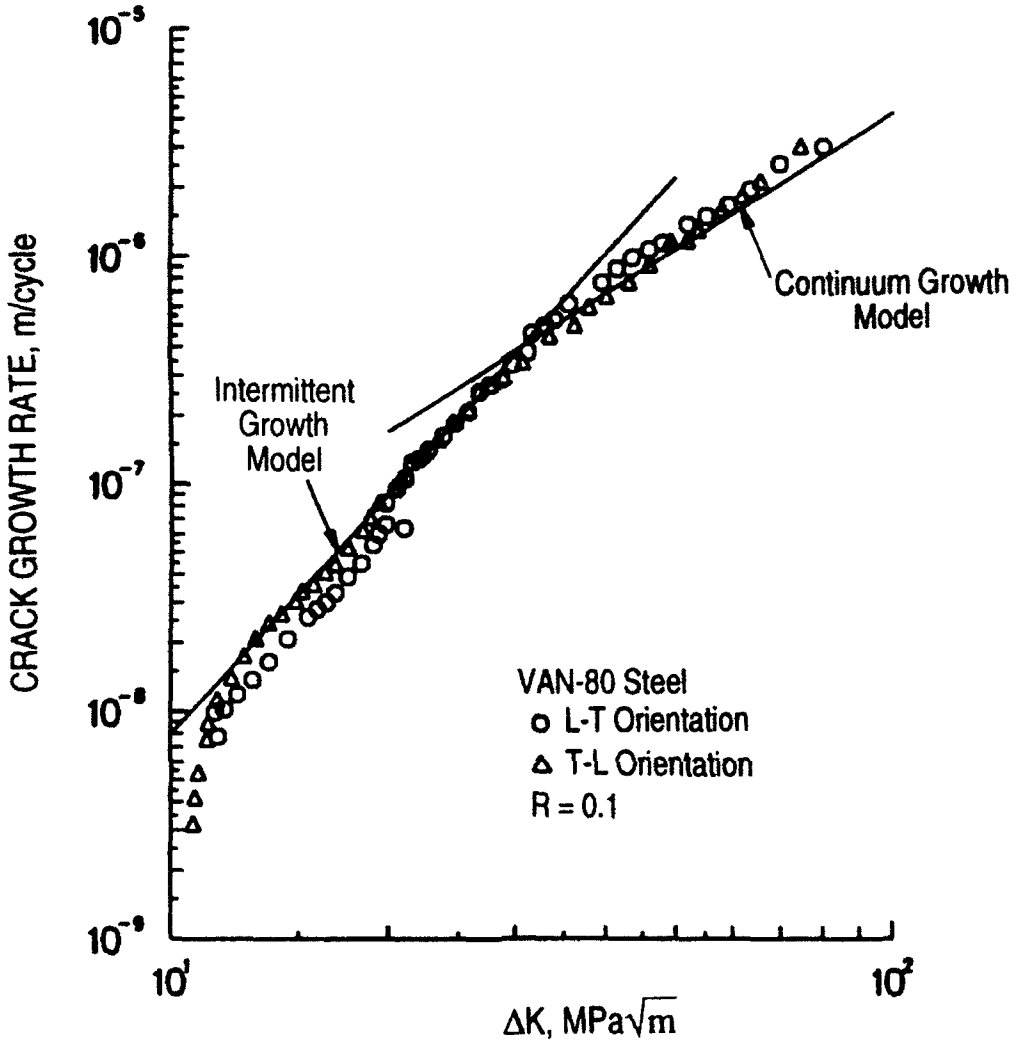

Figure 7. Comparison of model calculation with experimental data of VAN-8C steel from Hertzberg and co-workers [49,50].

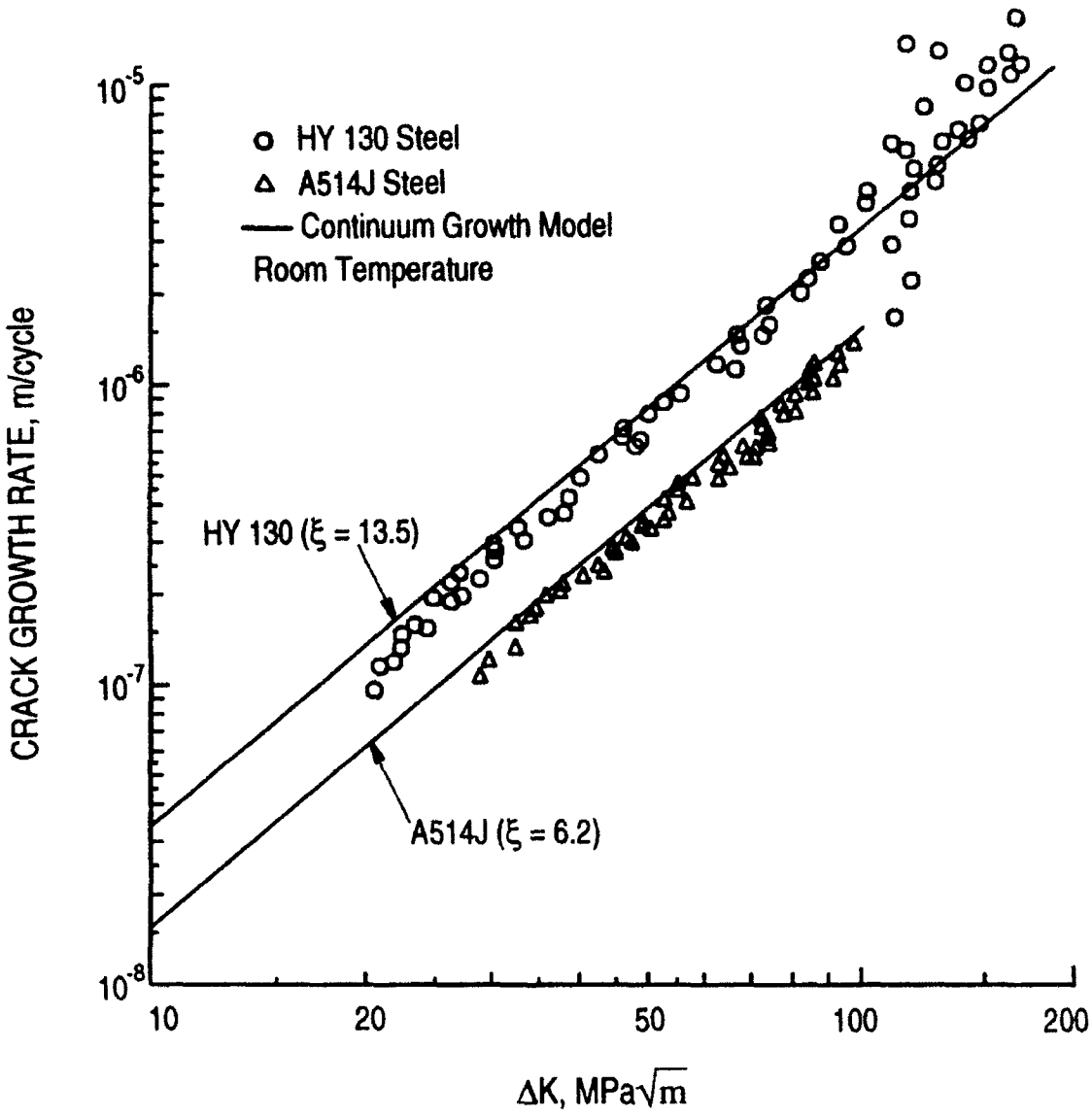

Figure 8. Comparison of model calculation with experimental data of HY130 [51] and A514J [52] steels in the continuum growth regime.

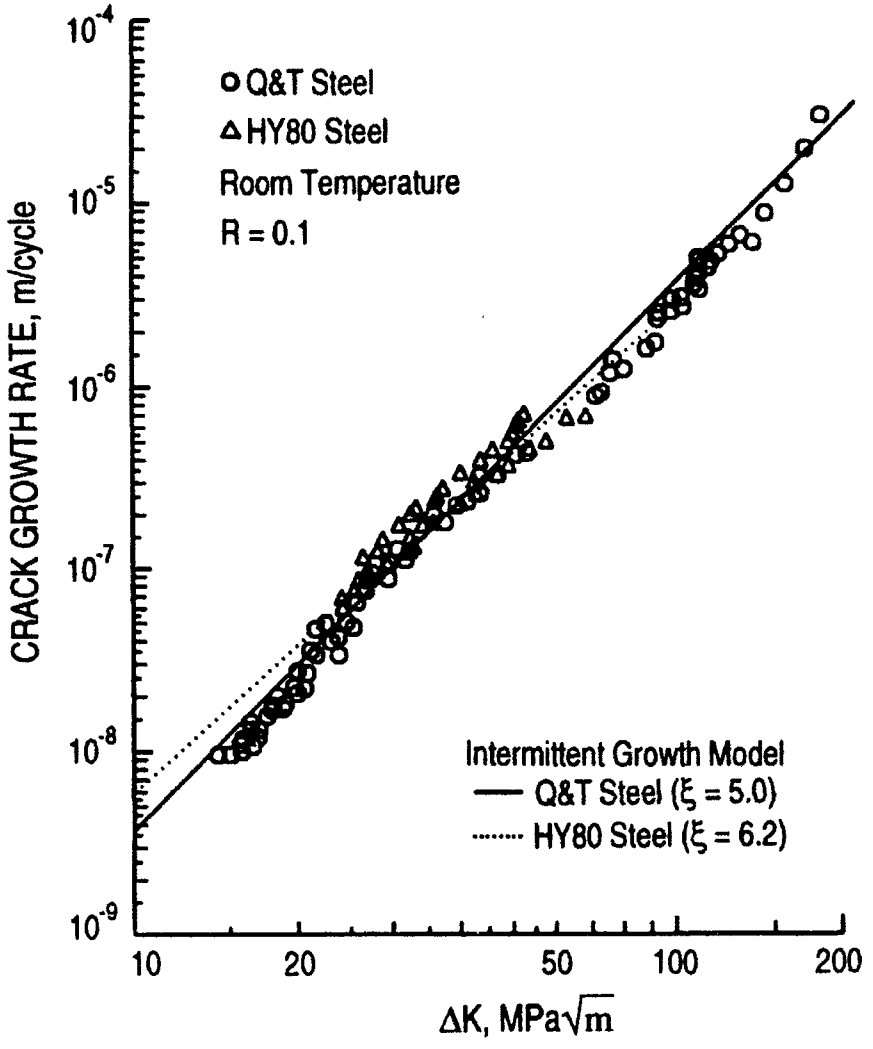

Figure 9. Comparison of model calculation with experimental data of HY80 [48] and Q&T steels [50] in the intermittent growth regime.

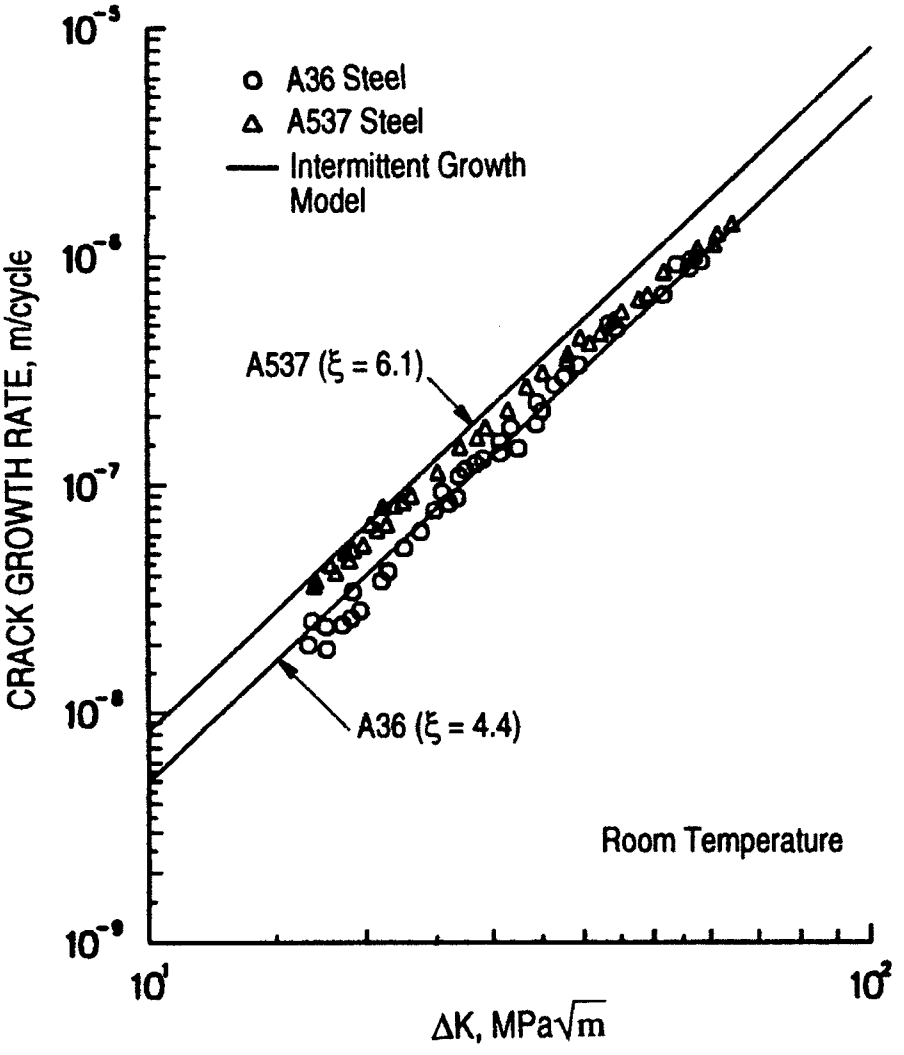

Figure 10. Comparison of calculated and experimental da/dN curves for A36 and A537A steels [46].

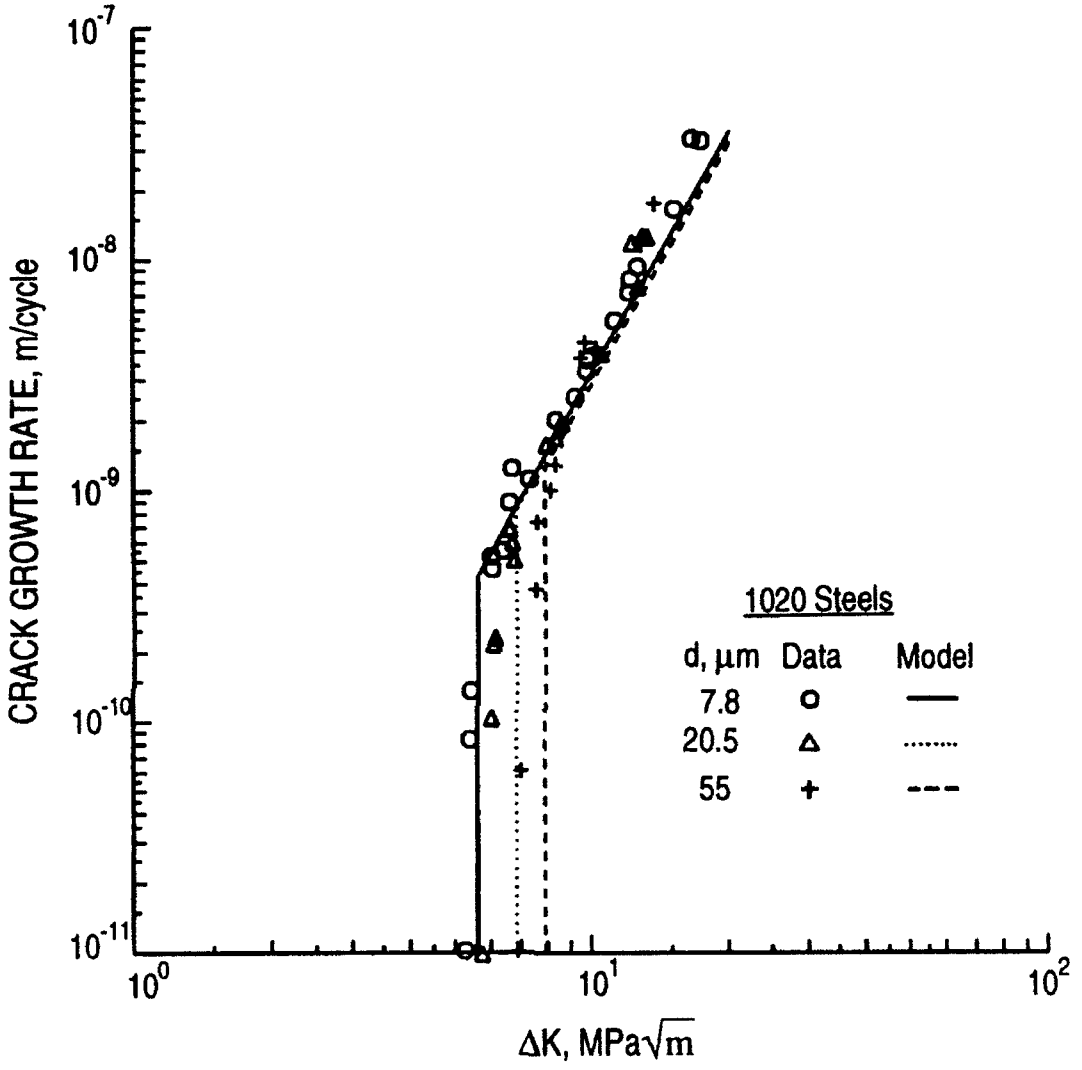

Figure 11. Calculated da/dN vs. ΔK curves compared to experimental data of 1020 steels. Experimental data are from Taira, et al. [45].

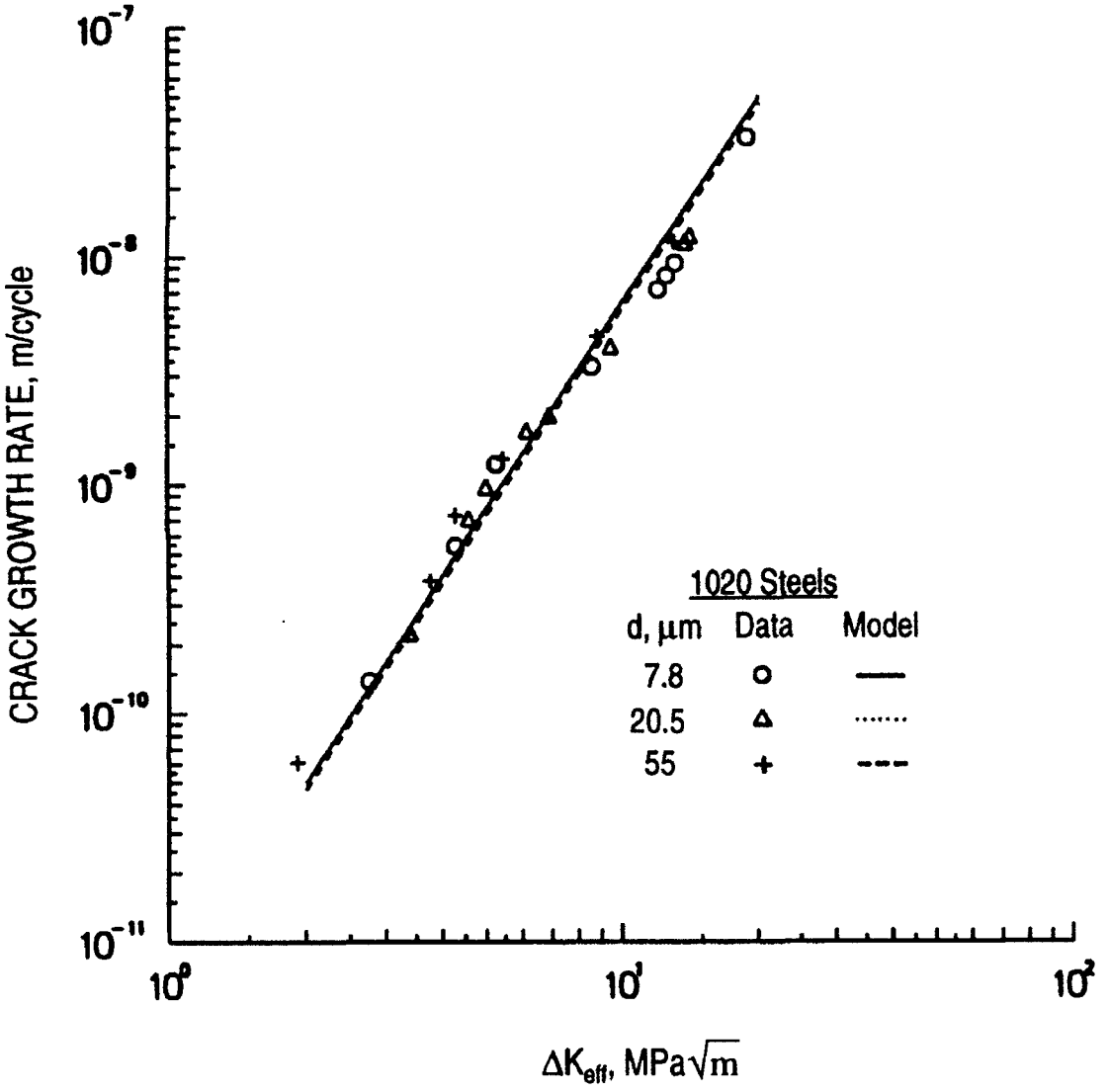

Figure 12. Calculated da/dN vs. effective ΔK curves compared to experimental data of 1020 steels. Experimental data are from Taira, et al. [45].

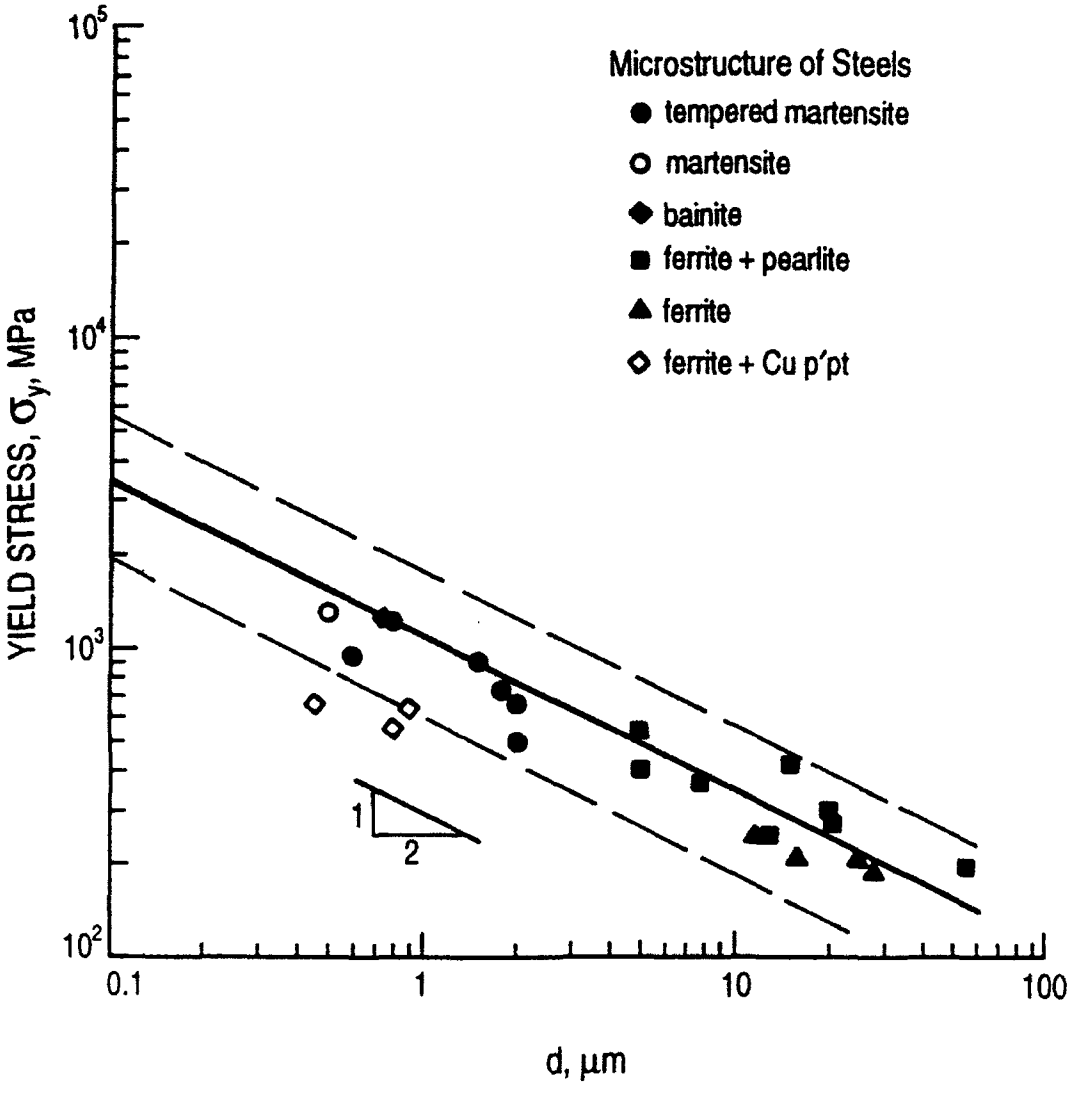

Figure 13. Dependence of yield stress on dislocation barrier spacing, d.

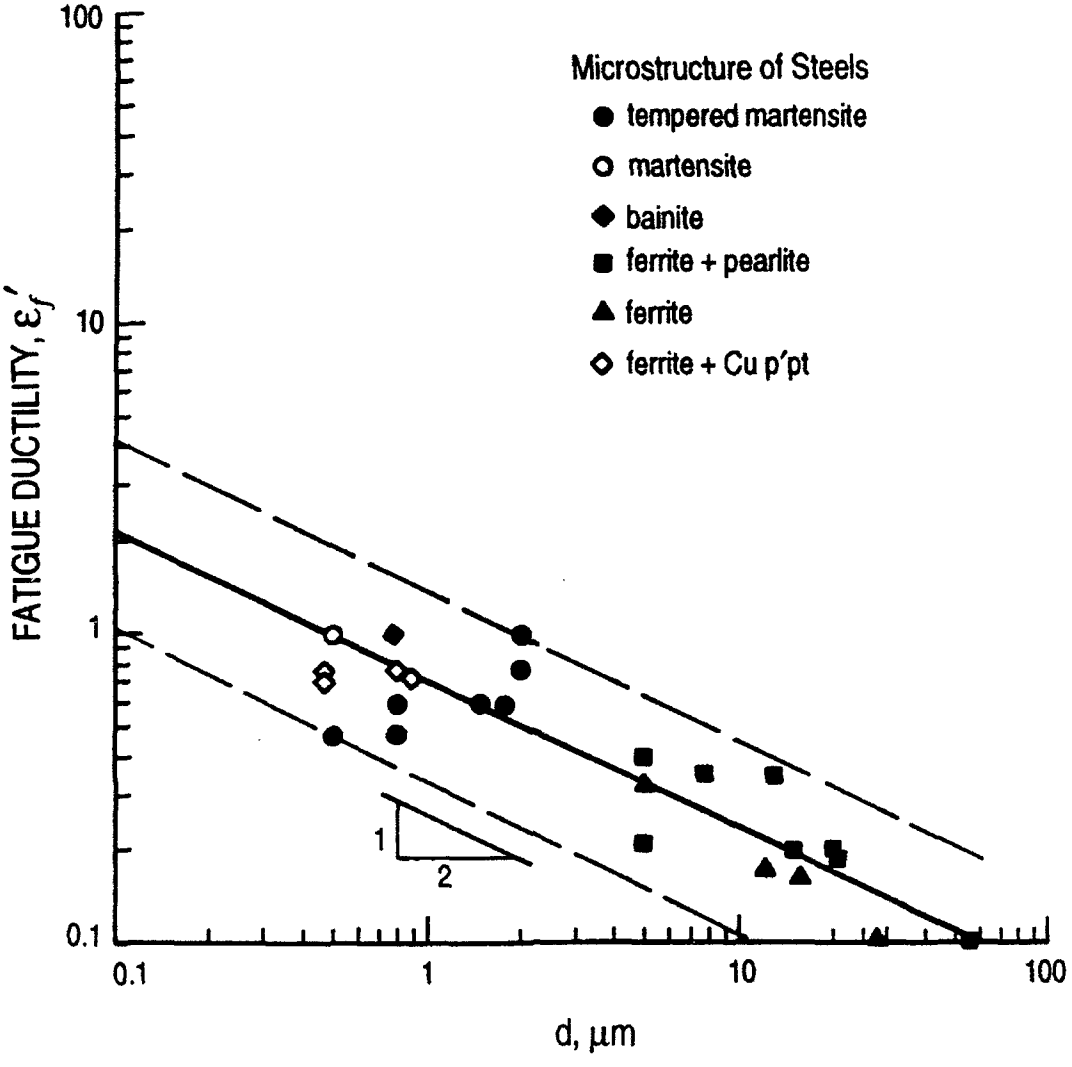

Figure 14. Dependence of fatigue ductility on dislocation barrier spacing, d.

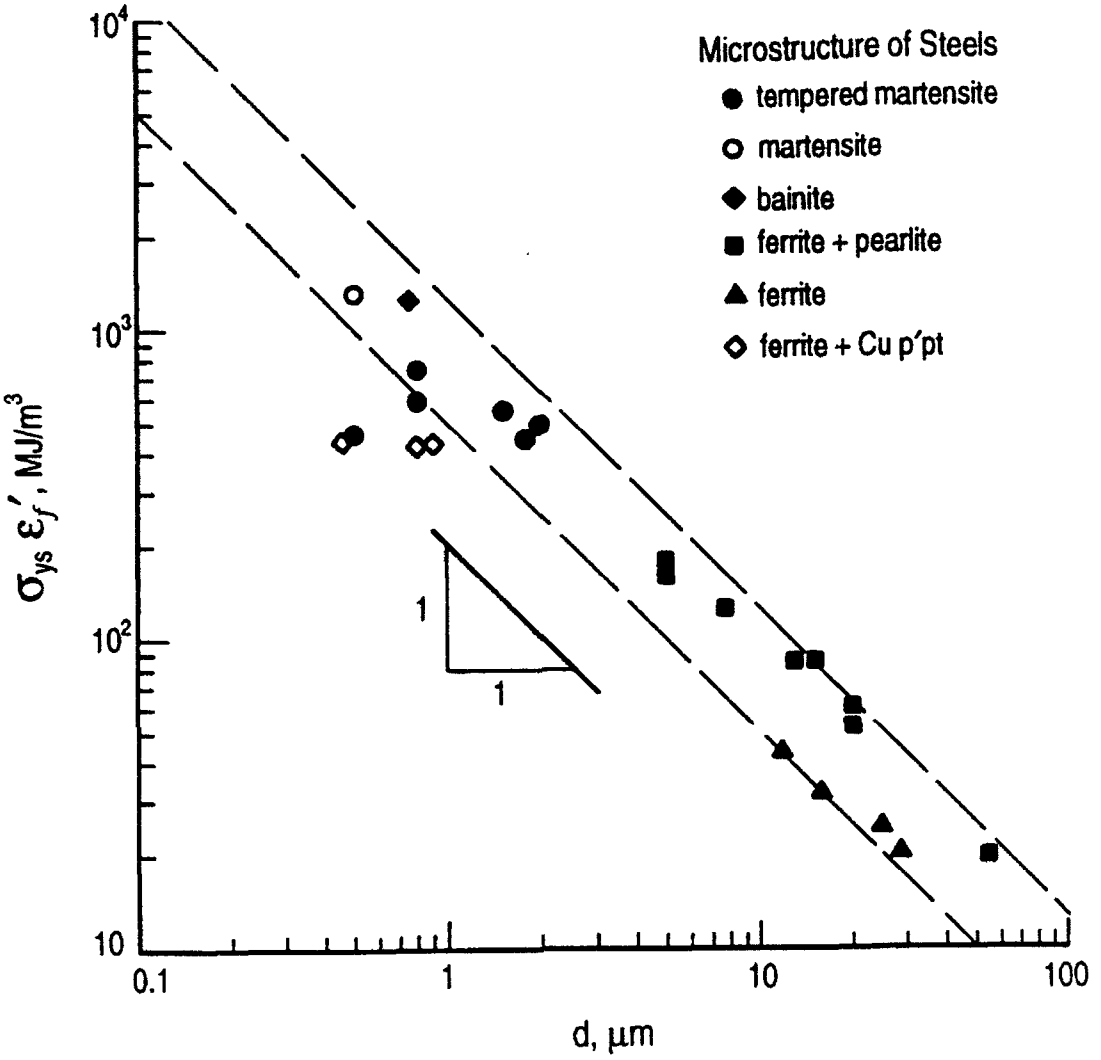

Figure 15. Dependence of $\sigma_y\varepsilon_f'$ on dislocation barrier spacing, d.

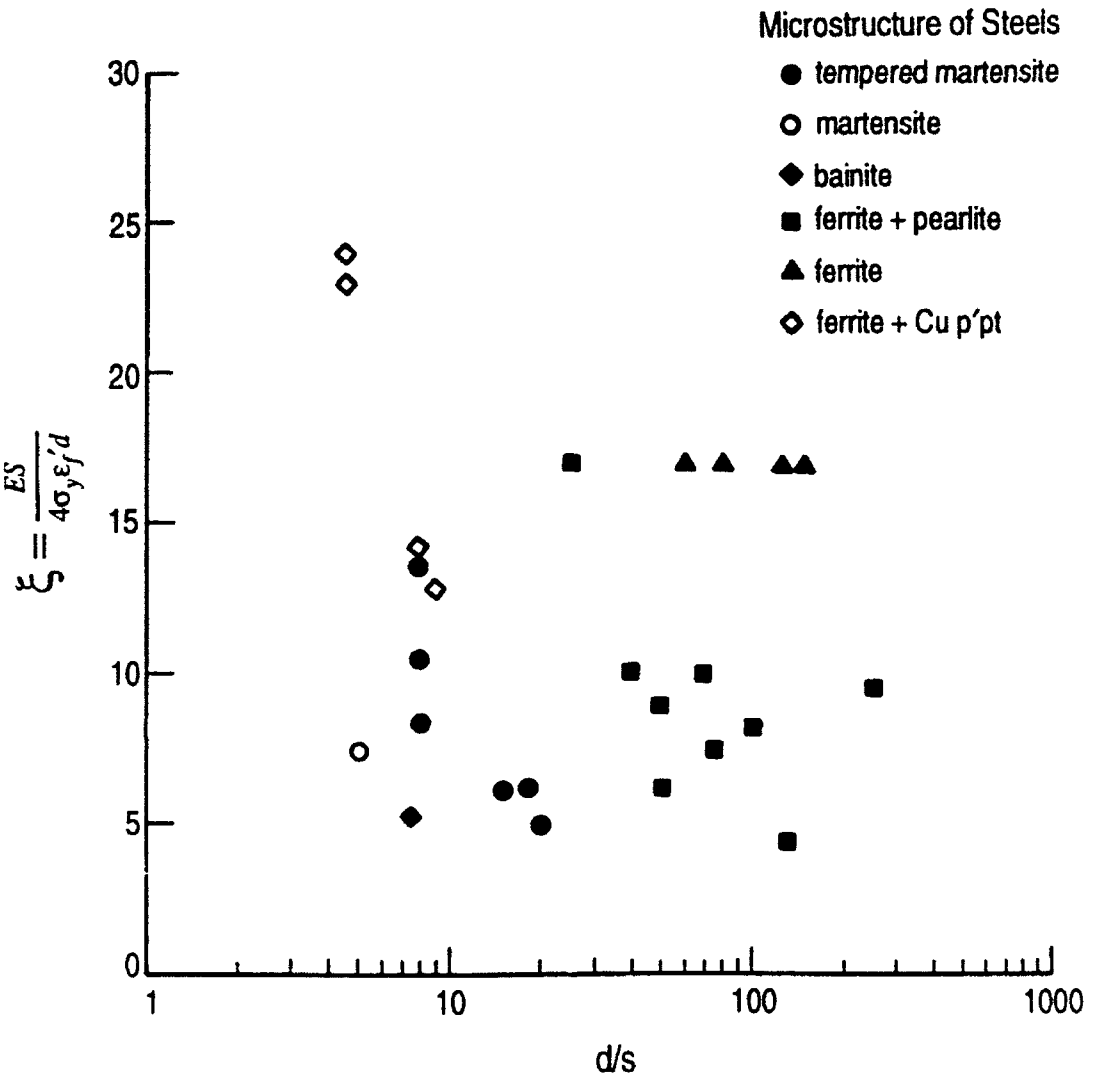

Figure 16. The lack of dependence of the dimensionless microstructural parameter, $\xi = Es/\sigma_y \varepsilon_f' d$, on the ratio of dislocation barrier spacing to dislocation cell size, d/s.

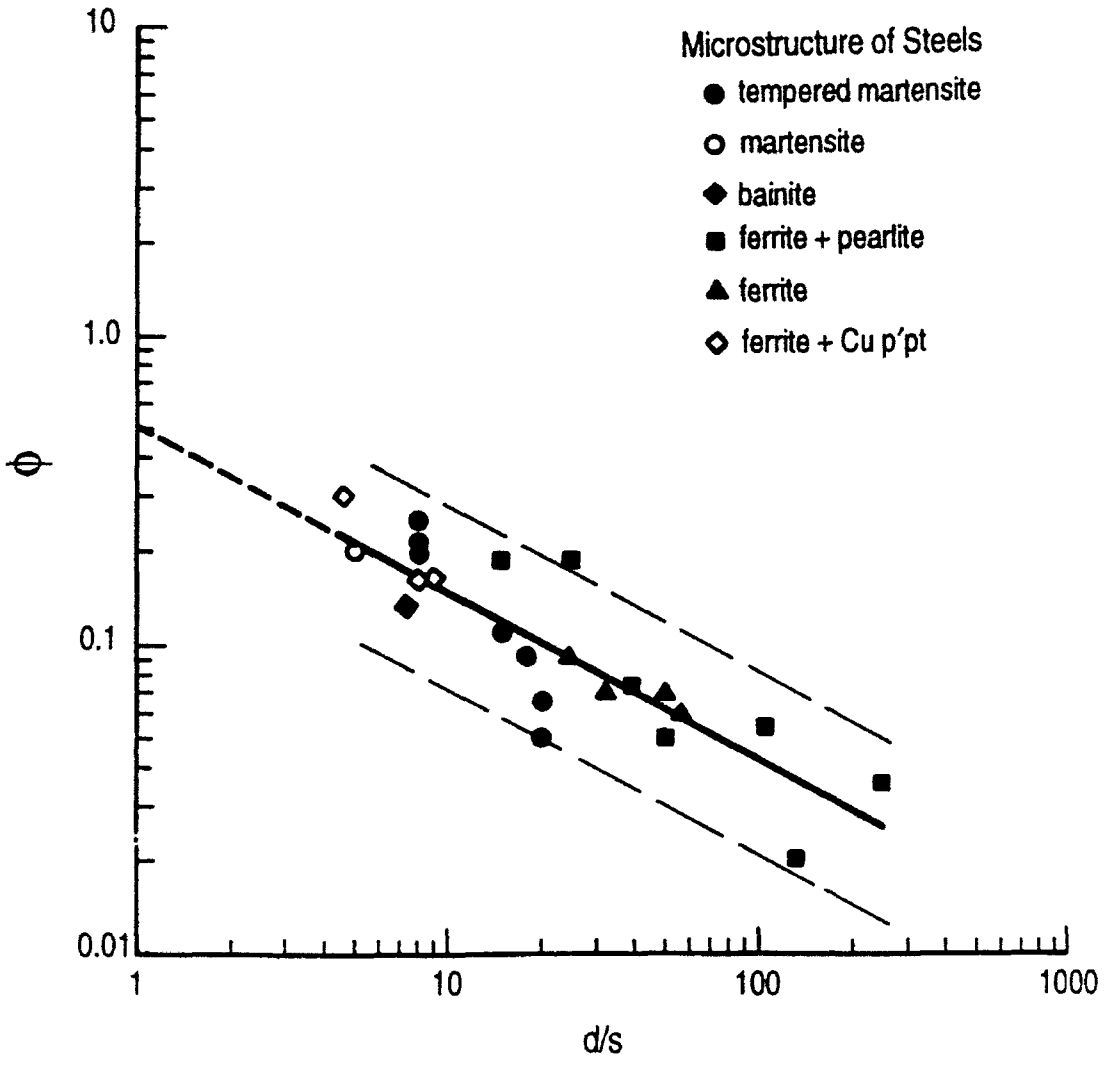

Figure 17. The dependence of the dimensionless microstructural parameter, $\phi = s/(\varepsilon_f' d)$, on the ratio of dislocation barrier spacing to dislocation cell size, d/s.

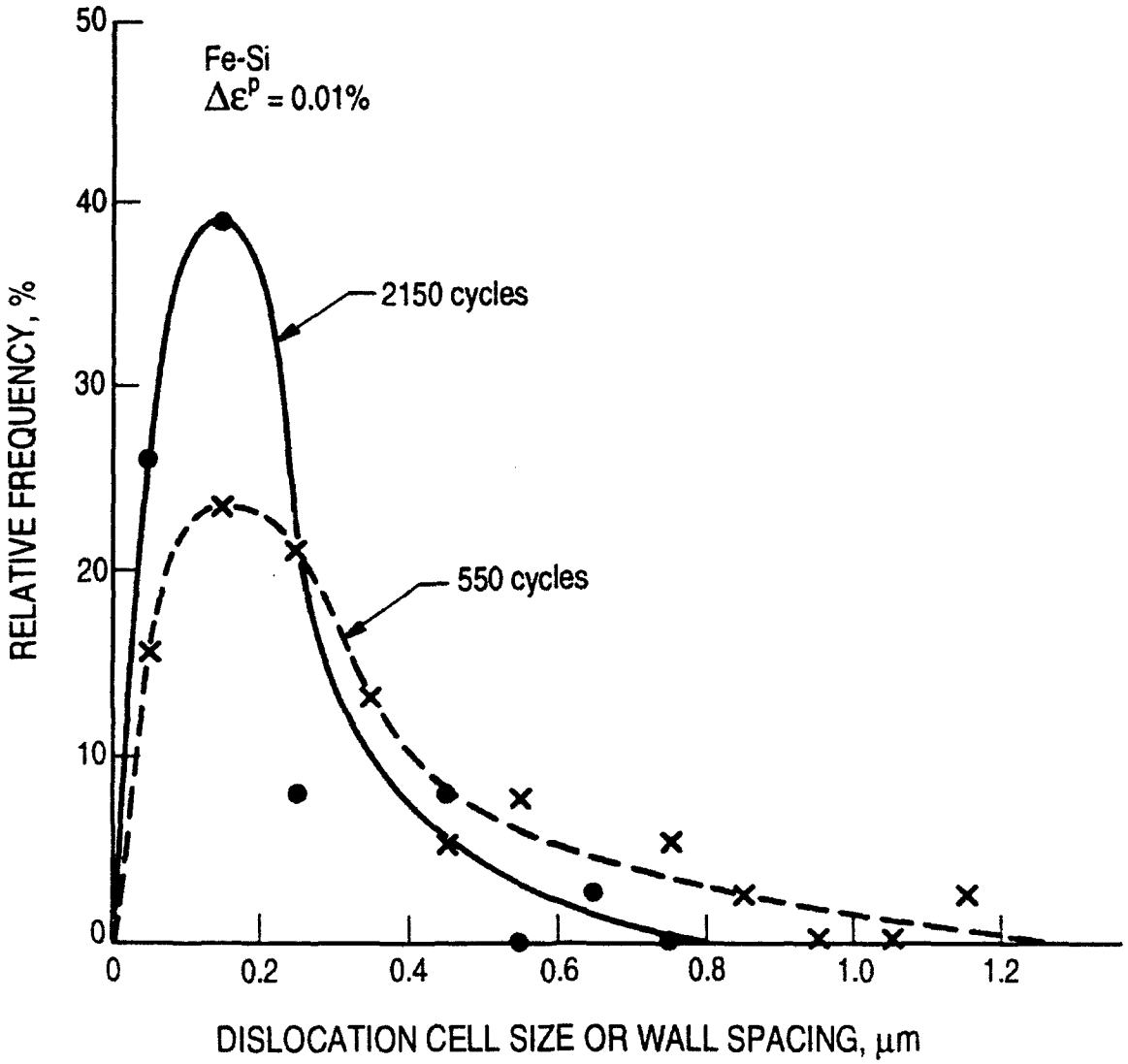

Figure 18. Distribution of dislocation cell size showing refinement of cell size with increasing fatigue cycles. Based on results of Keller, et al. [68].

Table I. Summary of yield stress (σ_y), fatigue ductility (ε_f'), dislocation barrier spacing (d), cell size (s), fatigue ductility exponent (b), crack growth exponent (m), and the dimensionless microstructural parameters ϕ and ξ for various steels. The parenthesized values for b and m correspond to values used in the continuum growth regime, while the unparenthesized values are for the intermittent growth regime. The relevant microstructures and the characteristic length corresponding to the dislocation barrier spacing, d, for individual steels are indicated in the last two columns.

Steel	σ_y, MPa	ε_f'	d, μm	s, μm	b	m = 2/b	ϕ	ξ	Microstructure*	Characteristic Length
HSLA-80 [43]	620.0	0.71 [40]	0.89 [33]	0.1	0.5 (1)	4 (2)	0.16	12.8	F + Cu precipitates	mean free path of Cu precipitates
(GAH) [27,40]	559.2 [40]	0.75 [40]	0.79 [33]	0.1	0.5 (1)	4 (2)	0.17	15.1	F + Cu precipitates	mean free path of Cu precipitates
(FZZ) [27,40]	633.0	0.71 [40]	0.46 [33]	0.1	0.5 (1)	4 (2)	0.31	24.2	F + Cu precipitates	mean free path of Cu precipitates
VAN-80 [49,50]	560.0	0.21 [50]	5 [50]	0.2	0.571 (1)	3.5 (2)	0.19	17.0	F + P	grain/colony size
HY80 [51]	655.0	0.77[c]	2[b]	0.1	0.65	3.1	0.06	5.0	tempered M	carbide spacing
HY130 [51]	965.3	0.48 [57]	0.8 [74]	0.1	(1)	(2)	0.26	13.5	tempered M	carbide spacing
A533B [11]	503.0	1.0[d]	2 [76]	0.1	(1)	(2)	0.05	5.0	tempered M	carbide spacing
A514J [52]	744.7	0.60 [57]	1.8[b]	0.1	(1)	(2)	0.09	6.2	tempered M	carbide spacing
10Ni-Steel [11]	1255.0	0.60 [57]	0.8[a]	0.1	(1)	(2)	0.20	8.3	tempered M	carbide spacing
Q&T Steel [50]	910.0	0.6 [57]	1.5 [50]	0.1	0.67	2.98	0.11	6.1	tempered M	carbide spacing
4340 [54]	1241.0	0.48 [57]	0.8[a]	0.1	0.6 (1)	3.33 (2)	0.26	10.5	tempered M	carbide spacing
4Cr-0-35C [53]	1324.0	1.0[d]	0.5 [8,59]	0.1	0.75	2.67	0.21	7.6	M	lath width

Table I (cont'd).

Steel	σ_y, MPa	ε_f'	d, μm	s, μm	b	m = 2/b	ϕ	ξ	Microstructure+	Characteristic Length
Ni-Mo-V Steel [11]	1240.0	1.0[d]	0.75[e]	0.1	(1)	(2)	0.13	5.4	B	carbide spacing
A36 [46]	248.2	0.35[d]	13 [56]	0.1	0.65	3	0.02	4.4	F + P	grain size
A537 [46]	406.8	0.40[d]	5 [56]	0.1	0.65	3	0.05	6.1	F + P	grain size
1020 [45]	366.0	0.35 [57]	7.8 [45]	0.2	0.571	3.5	0.07	10.0	F + P	grain size
	275.0	0.18[d]	20.5 [45]	0.2	0.571	3.5	0.05	9.9	F + P	grain size
	194.0	0.10[d]	55 [45]	0.2	0.571	3.5	0.04	9.4	F + P	grain size
0030 Cast Steel [47,48]	303.0	0.20[a]	20 [47]	0.2	0.5	4	0.05	8.3	F + P	grain size
0050A Cast Steel [47,48]	434.0	0.20[a]	15 [47]	0.2	0.5	4	0.07	7.7	F + P	grain size
Plain C Steel [44]	253.8	0.19 [58]	12 [44]	0.2	0.571	3.5	0.09	17.3	F	grain size
	211.7	0.19 [58]	16 [44]	0.2	0.571	3.5	0.07	15.5	F	grain size
	201.9	0.12[d]	25 [44]	0.2	0.571	3.5	0.07	16.5	F	grain size
	192.1	0.12[a]	28 [44]	0.2	0.571	3.5	0.06	15.5	F	grain size

+: F = ferrite; P = pearlite, M = martensite, B = bainite
a: estimated based on HY130 data
b: estimated based on Q&T steel data
c: estimated based on HSLA-80 data
d: fitted to crack growth rate
e: measured from SEM micrographs